PGV BASED NO-CODE MID-RISE REINFORCED CONCRETE FRAME-TYPE BUILDING FRAGILITIES IN İSTANBUL

by

Halil İbrahim Duran

B.S., Civil Engineering, Middle East Technical University, 2015

Submitted to the Kandilli Observatory and Earthquake Research Institute
in partial fulfillment of the requirements for the degree of
Master of Science

Graduate Program in Earthquake Engineering

Boğaziçi University

2020

ACKNOWLEDGEMENTS

I would like to thank my supervisor Prof. Dr. Sinan Akkar for his invaluable guidance and assistance throughout the study.

I would also like to thank my colleague İpek Dolağan for her friendship and contribution to this thesis.

Finally, I would like to express my deepest appreciation to my family for their endless support, understanding and love throughout my life.

ABSTRACT

PGV BASED NO-CODE MID-RISE REINFORCED CONCRETE FRAME-TYPE BUILDING FRAGILITIES IN İSTANBUL

16 building models representing a building stock in the Zeytinburnu District in İstanbul that includes approximately 800 mid-rise reinforced concrete (RC) frame buildings are used to develop PGV based fragility models that could partially represent the no-code building vulnerability in Turkey. The 3-D analytical models of the subject frames are modeled with distributed plasticity using the Open System for Earthquake Engineering Simulation (OpenSees) software. The damage states of the fragilities are determined by use of the performance limits of structural members from 2018 version of the Turkish Building Earthquake Code and 2005 version of the Eurocode 8. Peak ground velocity (PGV) is preferred as seismic intensity measure since it has a better correlation with deformation demands. 25 real ground motion pairs are selected using disaggregation results of three different PGV hazard curves determined from three ground motion predictive models that are used in the development of the most recent national seismic hazard maps. Response statistics are kept through incremental dynamic analysis (IDA) to develop fragilities for each model. The fragilities computed from above comprehensive nonlinear response history analyses advocate that consideration of variabilities in (a) structural models, (b) ground motion records and (c) limit states makes a huge impact in the exceedance probabilities of damage states. Therefore, a backbone fragility model, which covers the above uncertainties by up and down scaling of a central model is a must in proper loss assessment of building stocks.

ÖZET

İSTANBUL'DA YER ALAN VE YÖNETMELİKLERE UYMAYAN ORTA KATLI BETONARME ÇERÇEVE BİNALARIN MAKSİMUM YER HIZINA BAĞLI KIRILGANLIKLARI

Türkiye'de yer alan ve herhangi bir deprem yönetmeliğine göre tasarlanmamış binaların maksimum yer hızına bağlı hasargörebilirlilikleri kısmi olarak incelemiştir. Bu bağlamda İstanbul'un Zeytinburnu ilçesinde yer alan 800 adet orta katlı betonarme çerçeve binayı temsil eden 16 bina modeli kullanılmıştır. Binalar OpenSees (Open System for Earthquake Engineering Simulation) yazılımında 3 boyutlu olarak modellenmiştir. Binaların hasar durumları, 2018 yılında yayımlanan Türk Bina Deprem Yönetmeliği ve 2005 yılında yayımlanan Eurocode 8 yönetmeliğinde yer alan yapı elemanları hasar sınırları ile belirlenmiştir. Maksimum yer hızının elastik olmayan şekil değiştirme talepleriyle korelasyonu diğer yer hareketi indislerine göre daha iyi olduğu için, kırılganlık eğrileri maksimum yer hızına bağlı olarak çizdirilmiştir. İstanbul'un güncel deprem tehlike haritasının oluşturulmasında kullanılan 3 adet deprem tehlike eğrisinin deprem ayrıklaştırma sonuçları kullanılarak 25 adet deprem kaydı seçilmiştir. Bu kayıtlarla artımsal dinamik analiz formunda 3 boyutlu zaman tanım alanında doğrusal olmayan analizler yapılmış ve kırılganlık fonksiyonlarının geliştirilmesi için gerekli talep istatistikleri toplanmıştır. Yapılan kapsamlı analizler sonucu bir hasar durumunun aşılma olasılığını gösteren kırılganlık eğrilerinin oluşturulmasında (a) bina modellerindeki, (b) deprem kayıtlarındaki ve (c) hasar sınır durumlarındaki değişkenliklerin çok önemli etkilerinin olduğu sonucuna varılmıştır. Bu sebeple, bina stoklarının deprem kayıp tahminleri belirlenirken yukarıda sayılan değişkenlikleri kapsayan bir kırılganlık modelinin oluşturulması gerekir.

TABLE OF CONTENTS

LIST OF FIGURES

LIST OF TABLES

LIST OF SYMBOLS

α	Confinement effectiveness factor
β	Logarithmic standard deviation
ε	Ground motion error term
ε_c	Concrete strain
ε_s	Reinforcement strain
ζ	Critical damping ratio
η	Base shear coefficient
θ	Chord rotation
μ	Logarithmic mean
ρ	Ratio of reinforcement
ω	Mechanical reinforcement ratio of effective confinement
ϕ	Curvature
f_c	Concrete compressive strength
f_y	Reinforcement yield strength
g	Gravitational acceleration
J_{BR}	Joyner-Boore distance
M	Moment
N	Axial load
T_1	First-mode period
$(V_s)_{30}$	Shear wave velocities at 30 m below the top of the soil layer

LIST OF ACRONYMS/ABBREVIATIONS

2-D	Two dimensional
3-D	Three dimensional
ACI	American Concrete Institute
ASCE	American Society of Civil Engineers
DL	Damage limitation
DM	Damage measure
DPO	Dynamic pushover
DS	Damage state
cm	Centimeter
CD	Controlled damage
CP	Collapse prevention
DS	Damage state
FEMA	Federal Emergency Management Agency
EDP	Engineering demand parameter
EMS98	European Macroseismic Scale
GMPE	Ground motion prediction equation
HAZUS	Hazards United States
LD	Limited damage
LHS	Latin Hypercube Sampling
LS	Life safety
IDA	Incremental dynamic analysis
IM	Intensity measure
IO	Immediate occupancy
kN	Kilonewton
m	Meter
MDOF	Multi degree of freedom system
MIDR	Maximum interstory drift ratio
MLE	Maximum likelihood estimation
MMI	Modified Mercalli Intensity
MRF	Moment resisting frame

MSK	Medvedev–Sponheuer–Karnik
MPa	Megapascal
M_w	Moment magnitude
NBC	National Building Code of Canada
NC	Near collapse
NIBS	National Institute of Building Sciences
NRHA	Nonlinear response history analysis
NSP	Nonlinear static procedure
PBEE	Performance-based earthquake engineering
PEER	Pacific Earthquake Engineering Research
PGA	Peak ground acceleration
PGV	Peak ground velocity
PMF	Probability mass function
PSHA	Probabilistic seismic hazard analysis
R	Correlation coefficient
R^2	Coefficient of determination
RC	Reinforced concrete
s	Second
S_a	Spectral acceleration
SAC	Seismic Analysis Code
SD	Significant damage
S_d	Spectral displacement
SDOF	Single degree of freedom system
SEAOC	Structural Engineers Association of California
TBEC	Turkish Building Earthquake Code
TEC	Turkish Earthquake Code

1. INTRODUCTION

1.1. General

Turkey is one of the most quake-prone countries in the world since it has active fault zones and due to the high population density around fault zones, the country has suffered significant loss of life as well as economic losses with the actions of earthquakes during last decades. It is quite clear that these losses are due to the structural damage to the buildings during ground shaking. In recent years, in the course of rapid urbanization of the cities, buildings have been constructed with traditional techniques. This condition implies inadequate or no seismic design that ends up with structural damage under quake loads. Besides, since workmanship quality is inadequate, controlling mechanism is poor and unlicensed construction is popular around the country, earthquake loss, which can be defined as the decrease in the value of asset as a result of earthquake damage, is inevitable in this country.

Obviously, it becomes crucial to forecast potential social, environmental and economic results of future earthquakes. Earthquake risk assessment is a method to identify the nature and range of earthquake risk by investigating earthquake hazards and assessing present conditions of vulnerability that may harm people, services or the environment that they belong to. The purpose of earthquake risk assessment is to detect urban regions where huge economic and life losses are expected due to ground shaking. Results of such assessments are used to minimize expected life and economic losses by determining vulnerable buildings, deciding on strengthening or demolishing them and planning the rapid actions immediately after the earthquake. These studies increase awareness of people about the problem that they may encounter, help to detect common mistakes of construction techniques, encourage improving existed seismic design codes, and rise demand to earthquake-resistant structures.

Seismic hazard, fragility, and inventory of assets subjected to hazard are three significant factors for earthquake risk assessment (Erdik, 2017). Herein, the second ingredient, fragility analysis becomes important since it demonstrates the exceedance

probability of a certain damage state as a function of a ground motion parameter. Fragility curves can be accepted as a graphical notation of seismic risk (Rossetto and Elnashai, 2005) and may procure guidance to handle the mentioned issues. Fragility curves can be generated for a specific building or components of a building. Indeed, they can be generated for representative buildings of building stocks for the evaluation of the seismic vulnerability of regions. In this study, fragility functions are developed for no-code mid-rise reinforced concrete (RC) building stock in İstanbul. In this chapter, methods and components of fragility curves are explained. After summarizing notable relevant studies from the literature, the chapter is ended up with the objective and overall scope of the study.

1.2. Fragility Curve Methods

Fragility curves are a family of cumulative distribution functions that illustrate the probability of a specific building type (like low-rise RC frames in an urban region) exceeding or reaching a certain damage state (such as heavy damage or collapse) over a range of value of a ground motion intensity measure (preferably peak ground motion values). Therefore, generation of fragility curves requires characterization of ground motions as well as identification of different degrees of damages to the structures. Fragility curves differ according to the way of obtaining data necessary to plot them. Four common methods are being used in the generation of fragility curves: empirical, judgmental, analytical, and hybrid.

Empirical fragility curves use statistics of damage distributions of buildings acquired during post-earthquake surveys. Details like soil-structure interaction, topography, path, source and site characteristics are considered (Rossetto and Elnashai, 2003) in this method. Although it is realistic as it is based on observations, there are some difficulties in the application of collecting data. Since a limited number of large magnitude earthquakes exist on the areas with a high population, data came from observations stays scarce. Statistics are generally based on a few damage surveys, i.e., data is collected from a single location, or damage distributions are obtained on the strength of one earthquake. Consequently, generated curves become specific to a certain built environment with a particular geological property.

Judgmental fragility curves are based on estimations provided by earthquake engineering experts. It is time protective and economic but due to the dependence on the experience of experts, the reliability of the method is questionable.

Analytical fragility curves are based on the analysis result of structural models as a result of increasing seismic intensity. This method is practicable when there is no observational data from past earthquakes. In almost all cases, necessary data to develop fragility curves are obtained via computer programs. Modeling procedures can vary from elastic analysis of equivalent single degree of freedom (SDOF) systems to nonlinear response history analysis (NRHA) of 3-D systems. In this method, although it seems easy to model every kind of structure and generate data, there are some challenging parts like modeling of axial-flexure-shear interaction of the structural members, considering soil-structure interaction of the buildings or taking reinforcement buckling into account. In addition, convergence problems can be observed when large lateral forces are applied to the structure. It should not be forgotten that results of analysis depend dramatically on the element definition of structural models as well as the capabilities of computer programs.

The last method, hybrid approach is a combination of the other three methods. It aims to compensate for modeling deficiencies of analytical methods, subjectivity of earthquake engineering expert opinions and inadequacy of observational data.

1.3. Constituents of Fragility Curves

Fragility curves have three main constituents: identification of a building type, a ground motion intensity measure (IM) and a damage state (DS) definition. Damage estimations depend on the structural characteristics of the buildings. For this reason, a building classification that implies the starting point of fragility analysis is needed. Since construction methods differ among countries, or even among cities, fragility curves are region-specific. At this point, a building inventory study compiling building types, geometrical properties of the buildings, dimensions and detailing of structural members, as well as material information is necessary to make a general comment about the seismic performance of buildings at a specific region. Within this content, construction materials like structural steel, reinforced concrete, timber or masonry become important since they

directly affect yielding or collapse capacity together with the stiffness of the structural members. In addition, structural systems like moment-resisting frame, braced steel frame, or shear wall are substantial as the global stiffness and lateral load-carrying capacity of the structures change significantly among these systems. Another important parameter is the number of stories of the buildings. From observations of fields after severe ground shaking, it is understood that damage level rises with the increasing number of stories (Akkar et al., 2005). In the literature, regularity in plan or elevation, ductility, construction year, design code that is used for detailing of structural members of the buildings or existence of design code, as well as the change in material quality are also used for the building taxonomy.

Selection of a proper IM is the second constituent of fragility curves. It should be able to correlate well with the calculated or observed building damage. For the derivation of empirical fragility curves, common ground motion intensities are EMS98 scale (Grünthal, 1998), Modified Mercalli Intensity Scale (MMI) and MSK scale (Medvedev and Sponheuer, 1969). Spectral acceleration (S_a), spectral displacement (S_d), peak ground acceleration (PGA), and peak ground velocity (PGV) are the most common parameters in the derivation of analytical fragility curves. The advantage of using spectral quantities is that they are directly related to the building response. They give a fine estimation of response parameters, especially for the fundamental mode dominant buildings. However, for the evaluation of large building stocks, peak ground motion values can be preferred since they are period independent. For short period structures, PGA correlates well with the damage. For the structures in the intermediate period range like medium height buildings, PGV is a better damage indicator. It correlates well with deformation demands when compared to PGA and S_a (Molas et al., 2004).

The final element of developing fragility curves is the identification of a DS or a performance level. Performance levels can be named as immediate occupancy (IO), life safety (LS), and collapse prevention (CP) or none, minor, moderate, extensive and collapse, etc. in the literature. They are related to the limit values of engineering demand parameters (EDP). EDPs should be suitable for the determination of building response. Local or global EDPs exist for the evaluation of building response. Maximum interstory drift ratio (MIDR), maximum global drift ratio or roof displacement, Park and Ang damage

index (Park and Ang, 1985), final softening index, base shear, and story shear are widely used global EDPs in the literature. It should be determined considering building type and expected structural behavior of the buildings. To illustrate, if soft story vulnerability, which indicates existence of a weaker story than other stories in a building in terms of lateral load-carrying capacity, is expected for a building, global drift should not be chosen as EDP since it shows response of roof displacement of the building normalized by building height, rather than displacement of a story. MIDR, which means lateral displacement difference of two adjacent stories of the building normalized by the height of the story, is a good indicator of soft story mechanism. When local EDPs like strain, plastic rotation or chord rotation of the structural members are used, they should be converted to overall damage indices to evaluate general building response and generate fragility curves. When NRHA is carried out, the cyclic behavior of the structural members highly imprints the overall response of the building. Therefore, consideration of the DS definitions as a function of local members become highly important for fragility analysis.

An example of fragility curves is illustrated in Figure 1.1. which shows the probability of collapse of 3, 5 and 7 story reinforced concrete frame buildings designed according to the TEC (1975).

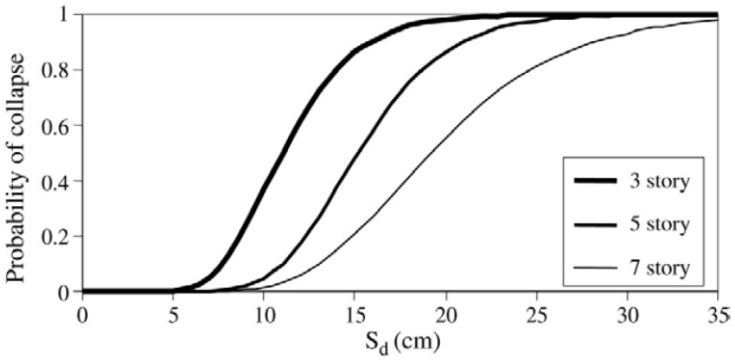

Figure 1.1. Collapse fragility curve for 3, 5 and 7 story buildings as a function of spectral displacement (Kırçıl and Polat, 2006).

1.4. Literature Survey

There is a wide literature about seismic evaluations of structures via fragility analysis. This study mainly focuses on the generation of analytical fragility curves for building stocks via NRHA since it is the most detailed and realistic analysis type. In this context, several significant studies from the literature are summarized in this section.

Singhal and Kiremidjian (1996) generate analytical fragility curves for low-rise, mid-rise, and high-rise RC frames. 3-D representative building models having 2, 5 and 12 stories are designed according to The Structural Engineers Association of California (SEAOC, 1990). 2-D models using one section of each building are created. 100 samples of concrete compressive strength and reinforcement yield strength are determined using the Monte Carlo simulation technique (Rubinstein, 1981) to consider uncertainty in structural capacities. 100 artificial earthquake records consistent with 3 real firm site records are generated. 2-D NRHA is performed to calculate structural demands. Park and Ang damage index (Park and Ang, 1985) is used for the determination of 4 damage levels and fragility curves of different types of buildings are derived as a function of S_a.

Kırçıl and Polat (2006) generate analytical fragility curves for mid-rise RC frame buildings in İstanbul. Building classification is done concerning the number of stories. Typical 3, 5 and 7 story buildings that are symmetric in the plan in both principal directions and designed according to the TEC (1975) are used for the generation of fragility curves. Two different reinforcement classes are considered for each model. 2-D NRHA is carried out using 12 artificial ground motions. Incremental dynamic analysis (IDA) (Vamvatsikos and Cornell, 2002) is performed to determine the yielding and collapse capacity of the buildings. The yielding limit is defined as the first point where MIDR - S_a (T_1, 5%) curve becomes nonlinear. The collapse limit is defined as the point where dynamic instability occurs at a MIDR value less than 3%. Otherwise, the collapse limit is accepted as 3% MIDR and corresponding S_a (T_1, 5%). At the end, fragility curves in the form of lognormal distribution functions with two parameters are expressed in terms of PGA, S_d, and S_a. In addition, yield and collapse probability curves with 95% confidence level are expressed in terms of MIDR. The IO threshold value of MIDR is determined at

the point where there is 5% probability of yielding. Similarly, the CP threshold value of MIDR is determined at the point where there is 5% probability of collapse.

Akkar et al. (2005) generate fragility curves for low-rise and mid-rise ordinary RC frame-type buildings with masonry infill walls in Turkey using a hybrid approach. 32 sample buildings with 2, 3, 4 and 5 stories are selected from the Düzce building database. Capacities of the buildings are obtained from field data and NRHA is carried out to calculate their dynamic response. Lateral deformation, strength and stiffness capacities of the buildings are determined using pushover analyses. The limit states are determined in terms of global drift. Among the buildings with the same story number, median yield value of global drift and median ultimate value of global drift are assigned as the IO and CP limit respectively. The LS limit is taken as 75% of the CP limit. Using capacity curves, the buildings are converted to equivalent SDOF systems with the guidelines of FEMA-356 (2000). 82 ground motion records are used for NRHA of SDOF systems and seismic demands are calculated. At the end, fragility curves are expressed as a function of PGV since it correlates with deformation demands better than PGA.

Ghobarah et al. (1998) evaluate the seismic performance of an existing 3-storey RC frame building designed for gravity and wind loads only according to the American Concrete Institute 318-63 (ACI, 1963). Besides, the performance of a similar building designed for earthquake loads according to the NBC (1995) is investigated for comparison. 2 different sets of 200 artificial ground motion records are generated for soil and rock sites, and they are scaled to different PGA levels. Uncertainties in the material strength and cross-section dimensions are considered using coefficients and distributions provided by extensive studies from the literature. The Monte Carlo simulation technique (Rubinstein, 1981) is used for the determination of probabilistic response characteristics of subject buildings. The performances of the buildings are evaluated using 4 damage levels from the Park and Ang damage index (Park and Ang, 1985). The results show that maximum interstory drift and roof drift responses are high for the low-code frame and damage level is low for the new-code design frame. At the end, mean story and roof drifts corresponding to 4 damage index values are proposed.

Ay and Erberik (2008) develop analytical fragility curves for low-rise and mid-rise RC frame-type buildings compatible with Turkish construction practice. For this purpose, typical 3, 5, 7 and 9 story buildings are used. Buildings are classified as poor, typical and superior according to the expected building seismic performance based on post-earthquake surveys. The Latin hypercube sampling (LHS) method (McKay et al., 1979) is used for structural variability and material uncertainty. IO, LS and CP limit states in terms of interstory drift ratios are determined from pushover analysis based on the ductility capacity of the structures. 60 ground motions are selected and classified into 3 sets according to their PGV range. 2-D NRHA is performed for the derivation of fragility curves in terms of PGV.

Erberik and Elnashai (2004) generate analytical fragility curves for flat-slab structures which are popularly used in quake-prone regions but rarely found in the literature. A 5-story building that is symmetric in the plan and designed according to the American Concrete Institute 318-99 (ACI, 1999) is used. The concealed beam within the slab and the part of the slab promoting frame behavior are considered to reflect flat-slab behavior in nonlinear modeling and a 2-D structural model is created. Masonry infills are modeled as diagonal compression struts. 4 limit states are determined in terms of interstory drift ratios by use of local member performances via pushover analysis. For material uncertainty, 30 values of concrete compressive strength, column reinforcement yield strength, and beam reinforcement yield strength are determined using the Latin hypercube sampling (LHS) method (McKay et al., 1979). NRHA is carried out with 10 ground motion records. Each ground motion is scaled at 11 ground displacement values. Fragility curves are generated as a function of spectral displacement. In addition, the same building is converted to the moment-resisting frame, that is, conventional beams are used instead of slab-beams. The same methodology is used to generate fragility curves of moment-resisting frames. It is observed that flat-slab structures are more vulnerable under quake loads.

Sadraddin et al. (2016) generate analytical fragility functions for code-compliant lower high-rise RC buildings and investigate the effect of shear wall configuration on seismic performance. For this purpose, one moment-resisting frame (MRF) and three dual systems containing combinations of MRF and shear walls with different configurations in

the plan are used. Sample buildings have 12 stories and the same plan shape, i.e., 4 buildings have the same bay width and number. Generic buildings are designed considering gravity and wind loads as well as seismic actions assuming they are located in Los Angeles, California region and have stiff soil conditions. 16 real ground motion pairs are selected to consider ground motion uncertainty. MIDR is used as EDP and S_a (T_1, 5%) is used as IM. IDA (Vamvatsikos and Cornell, 2002) is performed with 0.1 g intervals of S_a (T_1, 5%) and fragility curves are derived based on IDA results considering three limit states: slight damage, moderate damage, and collapse. For slight and moderate damages, MIDR limits in the HAZUS MR4 (NIBS, 2004) for shear wall and non-ductile MRF buildings are used. For the collapse limit, MIDR limits are determined from median IDA curves. At the end, it is stated that adding shear walls to the lower high-rise buildings having 10 to 20 stories increases seismic performance and interior shear walls have better performance when compared to exterior shear walls.

Erberik (2008) generates analytical fragility curves for masonry buildings in Turkey. 140 urban buildings from Dinar (Afyon) database and 69 rural buildings from Zeytinburnu (İstanbul) database are examined for the evaluation of general characteristics of Turkish masonry buildings. Buildings are classified according to their number of stories, regularity in the plan, load-bearing wall material and length of the walls, as well as openings in walls. 6 plans are generated with the combination of regular-irregular plan shapes and 3 different wall geometries created considering their compliance with minimum conditions of the TEC (2007). These plans are duplicated to 1 to 5 story building models and with the use of 4 different wall materials, 120 models are created. Masonry walls are modeled considering their in-plane behavior neglecting their out-of-plane rigidities. Pushover analysis is performed in order to determine building capacities. For each model, 20 different material simulations are generated using the Latin hypercube sampling (LHS) method (McKay et al., 1979) to take material variability into account. Median values of 20 pushover analysis results are used to determine 2 limit states in terms of base shear capacity. The first limit state corresponds to the end of the linear elastic branch of pushover curves, and the second one corresponds to the point where maximum base shear force is observed through pushover analysis. 50 ground motion records are used in NRHA and structural demands are determined. PGA is selected as ground motion intensity measure since it is a good candidate for rigid and non-ductile structural systems. At the end,

fragility curves are generated for each model and differences between model fragilities are observed. As expected, structural damage increases with the increase in the number of stories and plan irregularity and, the decrease in the material quality and code compliance of wall geometry. Finally, derived fragility curves are used for damage estimation of masonry buildings after the 1995 earthquake in Dinar and a clear agreement is observed with the actual damage.

As observed from past studies, there is no single method in the generation of analytical fragility curves because of the uncertainties involved in each step like limit state definitions, analyses method, the computer program used, selection of IM, etc. There are two types of structural systems used for fragility analysis: SDOF and MDOF. SDOF systems are created by the bilinearization of capacity curves obtained from pushover analysis. Such a method is applicable to the first-mode dominant structures like low-rise and mid-rise buildings. It has a few parameters for model creation. For this reason, completion of the study takes less time in this method. However, analysis accuracy is restricted due to the inherent distinctness between the dynamic behavior of MDOF and SDOF systems. Analysis of 3-D systems gives the most accurate responses because details like cyclic behavior of structural members, plan and elevation irregularity or soft story mechanism can be considered in this method. Usually, 2-D models are used for fragility analyses due to modeling complexity and analysis time of 3-D models. 2-D models are generally created using one section of the buildings. It gives similar responses with 3-D models when the structure is symmetric in the plan. But symmetric systems are rarely found in real buildings.

Generic models are generally selected from real existing buildings to represent building stocks. In addition, typical buildings having conformable plan configurations and section dimensions with existing buildings are created and detailed according to the design codes specified for the target region to be used in vulnerability studies. To consider uncertainties in material quality, plan configuration, section dimensions, etc., sampling techniques like the Monte Carlo simulation (Rubinstein, 1981) and the LHS method (McKay et al., 1979) are popularly used. For ground motion variability, a high number of earthquakes compatible with the geological conditions of the target region are used in NRHA. Artificial records are generated when a limited number of earthquake records exist.

For limit state definitions, using a damage index like Park and Ang index (Park and Ang, 1985) is popular. Some worthwhile studies like HAZUS MR4 (NIBS, 2004) provide limit states for building types and it is practical to use these definitions. In addition, pushover analysis or IDA (Vamvatsikos and Cornell, 2002) is popularly used for limit state definitions in terms of a global parameter like MIDR for the derivation of fragility curves.

1.5. Objective and Scope of the Thesis

With the cheapness and availability of the construction material and the simplicity of the application of the construction, RC becomes the most preferred construction technique across the world. In Turkey, mid-rise RC MRF buildings occupied as commercial or residential purposes are widely used. The ones constructed during fast urbanization of the cities after the 1960s do not meet with seismic design codes and so, do not have adequate lateral load-carrying capacity. Therefore, for this country, the abovesaid building type is considered as one of the most vulnerable ones under seismic actions.

This thesis focuses on generating fragility functions for no-code mid-rise reinforced concrete frame-type buildings in İstanbul. For this purpose, an inventory study from the Zeytinburnu District in İstanbul that includes 16 building models representing approximately 800 existing mid-rise RC MRF buildings are used. Subject buildings are constructed before 1980. They are not designed according to a seismic design code and supervision in the construction period is inadequate. So, they can be classified as no-code. 5-story building models are created considering structural model variability of the subject building type. The frame buildings are classified as Type-1 and Type-2 according to the existence of confinement mechanism in the structural members and satisfiability of minimum reinforcement detailing of the structural members with the TEC (1975).

3-D analytical building models are created using 3.0 version of the OpenSees (UC Berkeley, 2019) software. The nonlinear behavior of the structural members is identified using distributed plasticity. Incremental dynamic analysis, or simply IDA proposed by Vamvatsikos and Cornell (2002) is applied to those buildings by use of 25 real ground motion pairs. Ground motion pairs are selected from the PEER Strong Motion database (http://peer.berkeley.edu) based on disaggregation results of 3 different site-specific

seismic hazard curves developed for İstanbul. Through IDA, PGV of ground motions is monotonically increased with 2.5 cm/s intervals. Global (interstory drift ratio, top displacement and base shear of the building models) and local (rotation, strain and internal force of structural members) EDPs are recorded at each NRHA.

PGV is selected as seismic intensity measure since it correlates well with inelastic displacement demands (Akkar at el., 2005). The IO, LS, and CP performance limits are determined using strain limits from the TBEC (2018) and chord rotation limits from the Eurocode 8 (2005). Shear failure of local members and stories are considered with the guidelines of given two codes. At the end, fragility curves in the form of lognormal distribution functions with two parameters (logarithmic mean and logarithmic standard deviation) are generated for the target building stock considering structural model variability, limit state uncertainty and ground motion variability.

2. STRUCTURAL SYSTEMS AND GROUND MOTION SELECTION

2.1. Description of Building Models

Outcomes of a detailed inventory study published by Dolağan (2019) is used in order to generate fragility functions for no-code mid-rise RC MRF buildings in İstanbul. The blueprints of 800 existing RC residential buildings that are constructed before 1980 in the Zeytinburnu distinct in İstanbul are examined. The variations in key parameters like plan geometry, story height, cross-section dimensions of structural components, their material properties, column end conditions, as well as presence of mezzanine or pent floor are considered to develop 16 representative building models to partially encompass the model variation of the investigated building type.

95% of the buildings are MRF-type and 69% of them have 5-story. Therefore, only 5-story MRF buildings are created. Rectangular story plans are generated considering a set of parameters like observed span number and dimensions, asymmetrical configuration of columns and unconstrained columns. Most observed values of story heights, plan dimensions and beam-column dimensions from the building inventory are used to create representative buildings. Story height is taken as 2.75 m for typical floors, 3.25 m for ground floors without mezzanine floor and 5.5 m for ground floors with mezzanine floor. 45/35 cm column dimensions and 20/50 cm beam dimensions are used for the generation of representative buildings. The mean value of the concrete compressive strength of existing buildings (11 MPa) is used for generic models and reinforcement yield strength is taken as 220 MPa since it is the same for all 800 buildings.

There is no information about the reinforcement detailing of the building stock. For half of the models, minimum conditions of the TEC (1975) are used for the detailing of structural members and, confined concrete properties are used in nonlinear modeling. They are named as Type-1 buildings. For the other half, the buildings are named as Type-2 buildings and unconfined concrete properties are considered. The amount of longitudinal reinforcement is assumed as less than the minimum conditions of the TEC (1975) for Type-2 buildings. A considerable amount of differences is observed in terms of response

statistics of two building types that will be illustrated in the next sections of this thesis. Fragility curves are generated for each building type separately in Chapter 4.

2.2. Nonlinear Modeling

3-D finite element building models are created by use of 3.0 version of OpenSees (UC Berkeley, 2019) software. Columns and beams are modeled using the "nonlinearBeamColumn" element of the software. This command considers distributed plasticity along with the line elements. Five integration points are assigned to the columns and beams, and element deformations are calculated by integrating section internal forces at each integration point using the Gauss-Radau rule (Jamei et al., 2005) within the software. The cross-sections of the structural components are divided into several numbers of fibers (20x20 fibers for core concrete, 10x10 fibers for cover concrete, 1 fiber for each longitudinal reinforcement). The "Concrete04" material of the software which is identical to the concrete model proposed by Mander et al. (1988) is used to define compressive stress and strain relationships of core and cover concrete. The tensile strength of concrete is taken as 0. For reinforcement model definition, the "Steel02" material command that is developed according to Menegotto and Pinto (1973) is used for the hysteretic behavior of reinforcement. All material models used in this study are illustrated in Figure 2.1.

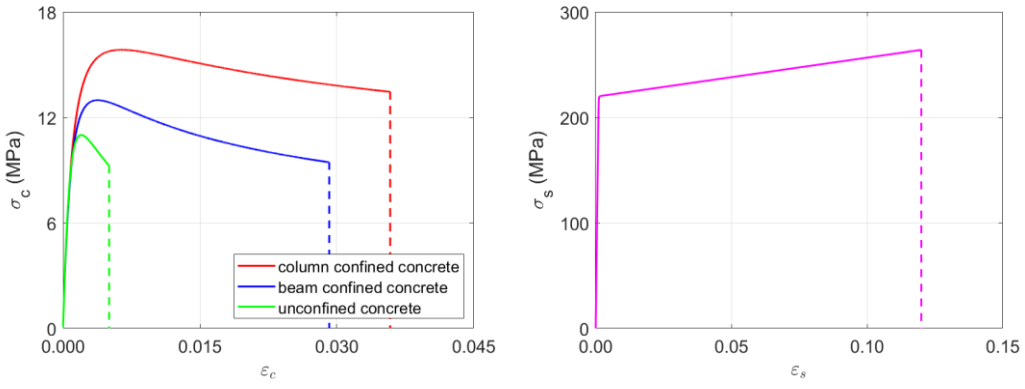

(a) Concrete (b) Reinforcement

Figure 2.1. Material stress-strain relationships.

Using fiber sections, hysterical properties of structural components are defined by concrete and reinforcement material properties. There is no need to define moment-

curvature relationships and moment-axial load interaction surface of the structural members which are shown in Figure 2.2, Figure 2.3 and Figure 2.4. They are directly included in the analyses by defining material properties for each fiber. For columns and beams with confined concrete properties, the moment capacity is higher and more ductile behavior is observed in these figures. Column and beam sections are assumed as elastic in terms of torsional and shear behavior. They are defined independently from fiber sections and assigned to fiber sections using the "section Aggregator" command. There is no interaction between shear, torsion and flexure behavior of structural members in this study. Slabs and foundations are not modeled as structural members. The self-weight of slabs is included in gravity analysis. The joints at each floor level are constrained by the rigid diaphragm assumption. The columns are fixed for all degrees of freedoms at the foundation level.

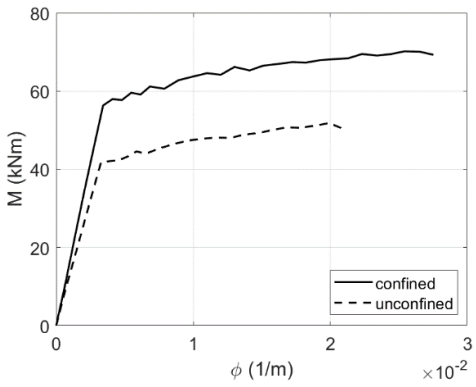

Figure 2.2. Moment curvature diagram of beams with confined and unconfined concrete.

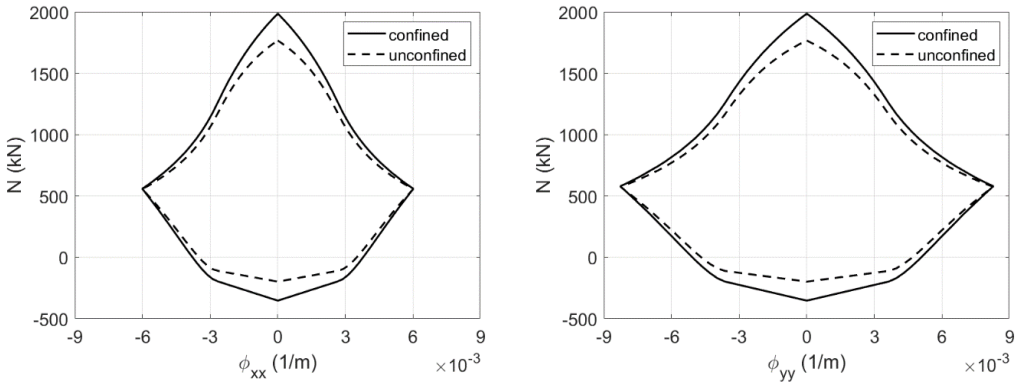

Figure 2.3. Axial load – yield curvature interaction diagram of columns with confined and unconfined concrete in both principal directions.

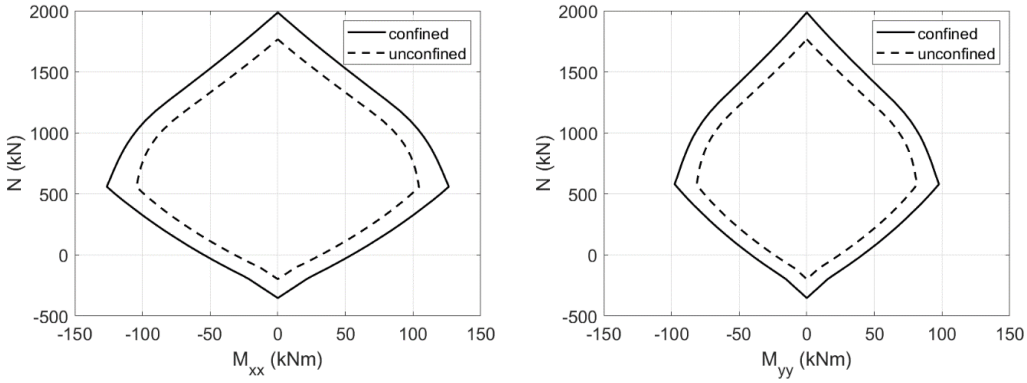

Figure 2.4. Axial load – yield moment interaction diagram of columns with confined and unconfined concrete in both principal directions.

Floor masses are calculated with the combination of dead load and 30% of the live load. Masses are assigned to the nodes at each story level. Dead load is taken as 4.5 kN/m^2 including self-weight of slabs. Live load is taken as 2 kN/m^2. For the consideration of the effect of gravity loads on the structures that are displaced laterally, P-Δ effects are included in the analyses. It is a way of defining geometric nonlinearity through NRHA. This condition increases structural responses like story drifts and may contribute to the dynamic instability. NEHRP Seismic Design Technical Brief 4 (Deierlein et al., 2010) recommends equivalent viscous damping in between 1% and 5% of critical damping over the range of elastic periods from 0.2T to 1.5T. Therefore, in order avoid overdamping during NRHA, critical damping ratio is accepted as 2.5% for each mode.

Based on the above definitions, 16 building models are created via OpenSees (UC Berkeley, 2019) in order to conduct gravity analysis, free vibration analysis, pushover analysis as well as NRHA in the form of incremental dynamic analyses or simply IDA proposed by Vamvatsikos and Cornell (2002).

2.3. Pushover Analysis

2.3.1. Description of Pushover Analysis

Pushover analysis, also known as the nonlinear static procedure (NSP) is a simple and approximate methodology to estimate the inelastic performance of structures under seismic loads. The assumption behind pushover analysis is that inelastic response of a complex MDOF system can be related to a simple equivalent SDOF system response. Pushover analysis starts with applying a predefined lateral load distribution to a building structure. The load distribution is constant along with the height of the building and applied to each story. The lateral load is raised until the yielding of a structural member. At this point, the overall stiffness of the building is modified considering the yielded member and the lateral load is again applied to the building until yielding of another structural member. This process goes on until the building model becomes unstable or a predefined target displacement is reached. At the end, a force-displacement curve (generally base shear versus top displacement) called capacity curve is plotted. Complex MDOF systems can be converted to simple equivalent SDOF systems by bilinearization of capacity curves with the guidelines of a given code like FEMA-356 (2000).

The maximum response of an equivalent SDOF system under earthquake loads can be correlated with the top displacement of a MDOF system. It is a preferable method for performance assessment of the structures under seismic loads since it is conceptually simple. In addition, the yielding or collapse of the structural members, stories or the overall building can be observed via pushover analysis and the overall lateral load-carrying capacity of the building can be estimated. Pushover analysis can be used for the identification of failure modes of the structures (like soft story mechanism or high axial force demands on brittle columns) or weak points of structural design procedure in the elastic analysis.

The procedure of pushover analysis comprises simplifications and approximations. For this reason, the reliability of the method is in debate among researchers. In pushover analyses, it is expected that the responses of the building components are similar to the ones obtained from NRHA. However, there are some valuable issues affecting the accuracy of the results of pushover analysis. The most important component of the analysis is the assumption of lateral load distribution. For traditional pushover analyses, the load pattern is assumed as invariant. Rectangular, inverted triangular or parabolic shapes are commonly used in recent studies. Distributions based on proportions of story mass or, proportions of the product of story mass with story displacement associated with the elastic first-mode shape are also used for nonlinear static analyses. These load patterns usually correspond to certain deformation modes. Therefore, potential failures due to the higher mode effects could not be predicted if first-mode based load distribution is used. In addition, the redistribution of inertia forces due to progressive yielding of structural members cannot be considered if invariant load patterns are used. A multi-modal load pattern can be used to consider higher mode effects and for the consideration of redistribution of inertia forces, an adoptive procedure can be followed by changing load distribution after yielding of structural members. But these procedures make pushover analysis computationally and conceptually complicated. In addition, it is still an issue that a static loading is applied to the structures whether it is invariant or adoptive and, a nonlinear dynamic response cannot be predicted by a static procedure with a high degree of accuracy. For this reason, generally invariant load distribution which is simple and effective is preferred among researchers.

2.3.2. Methodology and Results of Pushover Analysis

In this study, pushover analysis is used to determine base shear capacities of 16 building models and make a comparison of the results between nonlinear static analysis and IDA (Vamvatsikos and Cornell, 2002). Pushover analysis is performed for 16 building models by use of 3.0 version of OpenSees (UC Berkeley, 2019) software with the guidelines of TBEC (2018). An invariant lateral load distribution based on proportions of the product of story mass with story displacement associated with the first-mode shape is used. The 3-D building models are subjected to a monotonically increasing lateral load distribution. The analyses are carried out in both principal directions separately until global

instability is observed. Interstory drifts and its distribution along the building height is critical for the evaluation of the seismic performance of the buildings since it is a good indicator of damage under quake loads. For this reason, base shear coefficient versus maximum interstory drift ratio relationships of all 16 building models are plotted as capacity curves and, illustrated in Figure 2.5 in both principal directions of two building types. The importance of model variability in the same typology can be seen from these capacity curves. The base shear coefficient value (base shear force normalized by the building weight) of no-code RC MRF type buildings having 5 stories ranges from 0.05 to 0.13. For buildings having confined concrete mechanism, lateral strength and deformation capacities are explicitly higher. In addition, since the strong axis of 45/35 cm columns is along the x-direction, the buildings have higher capacity in the x-direction.

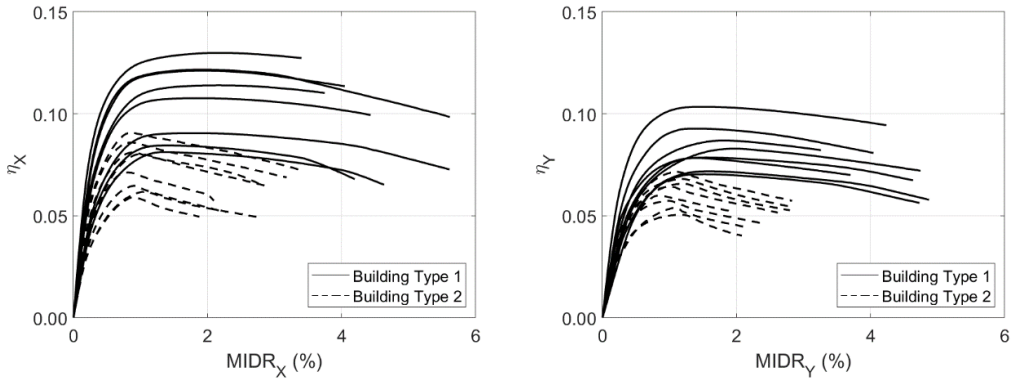

Figure 2.5. Pushover curve of 16 building models in both principal directions.

In addition to capacity curves, the relationship between the fundamental period and base shear capacity of the buildings is observed in both principal directions and shown in Figure 2.6. The figure illustrates that the fundamental periods of the building models range from 0.60 seconds to 1.35 seconds and it can be seen that as natural period increases, base shear capacity decreases. The spectral variations of the TEC (1975) and the TEC (1998) are also plotted on the same figure after converting spectral acceleration to base shear coefficient.

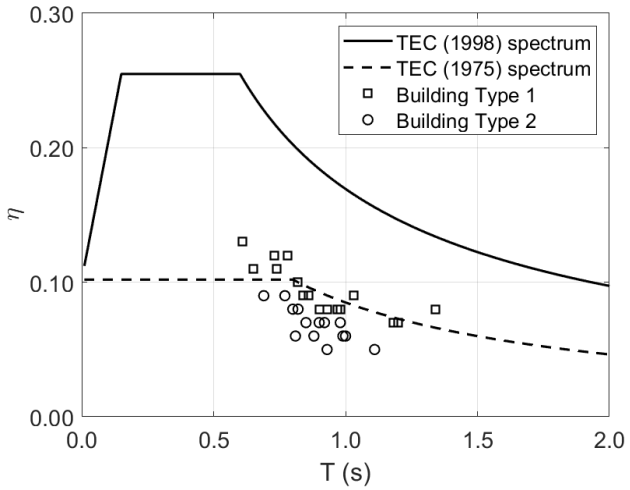

Figure 2.6. Effective period range of 16 building models with respect to base shear capacities in both principal directions.

The minimum base shear capacity of the TEC (1998), which is the updated version of the TEC (1975) is not satisfied for all buildings. Some of the Type-1 buildings having confinement mechanisms satisfy minimum base shear capacity of the TEC (1975). In all cases, the Type-2 buildings having unconfined concrete properties do not satisfy the minimum base shear capacity of the TEC (1975).

2.4. Ground Motion Data

2.4.1. Probabilistic Seismic Hazard Analysis

Probabilistic seismic hazard analysis (PSHA) is the integration of aleatory uncertainties like magnitudes and locations of future earthquakes in order to determine the mean annual rate of exceedance of given earthquake parameters at a specific site. Characterization of seismic sources, characteristics of earthquake occurrence for each source, ground motion prediction equation (GMPE) and seismic hazard quantification are basic ingredients of PSHA. It is carried out for the evaluation of the likelihood of occurrence at any level of ground shaking. The contribution of all the sources that can affect seismic activity is reflected via PSHA. Disaggregation of seismic hazard finds out the scenarios of earthquake driving the hazard at given levels of ground motions. Bins of

magnitude (M_w), distance (R) and often ground motion error term (ε) are used to characterize these scenarios (3-D disaggregation).

PSHA is significant for the selection of appropriate ground motion records to be used in NRHA of structures since characteristics of ground motions should be similar to those scenario events which are more likely to cause an exceedance of the target ground motion intensity level at a specific site (Barani et al., 2009). In this study, the results of a PSHA carried out by Prof. Özkan Kale for İstanbul is used for the selection of ground motions. The reference site has a shear wave velocity of 500 m/s which reflects stiff soil conditions in TBEC (2018). The ground motion prediction equations are KAAH15 (Kale et al., 2015), ASB14 (Akkar et al., 2014) and CY14 (Chiou and Youngs, 2014). These three different ground motion models encompass the ground motion model uncertainty in the derivation of fragility functions. The complete joint distributions of M_w-R-ε of three models are illustrated in Figure 2.7, Figure 2.8 and Figure 2.9.

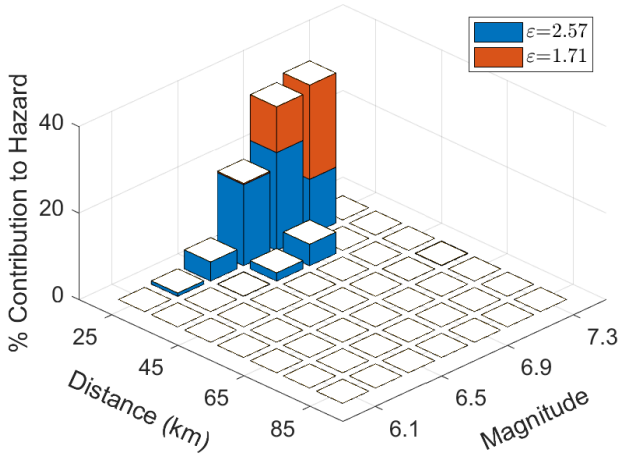

Figure 2.7. Joint M_w-R-ε probability mass functions (PMF) for İstanbul according to KAAH15 (Kale et al., 2015).

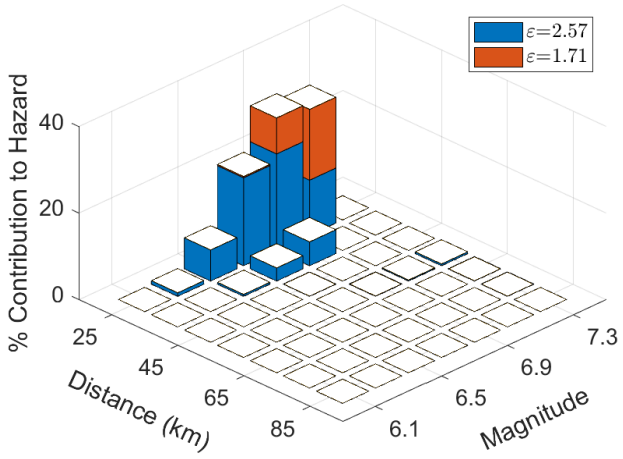

Figure 2.8. Joint M_w-R-ε probability mass functions (PMF) for İstanbul according to ASB14 (Akkar et al., 2014).

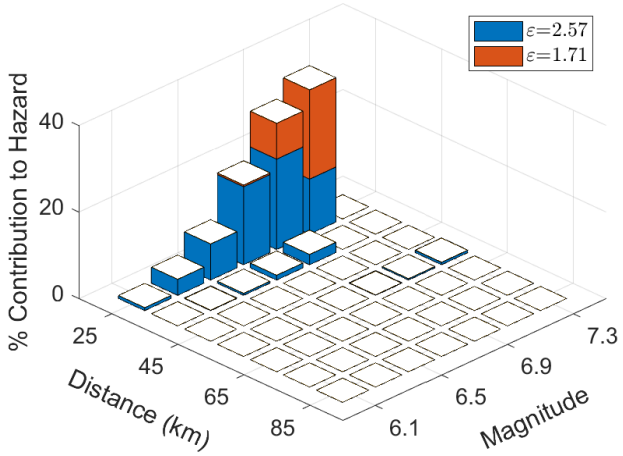

Figure 2.9. Joint M_w-R-ε probability mass functions (PMF) for İstanbul according to CY14 (Chiou and Youngs, 2014).

2.4.2. Characteristics of Selected Ground Motions

Vulnerability analysis of buildings subjected to seismic hazard is probabilistic due to ground motion record variability. It is much more important than material uncertainty for reinforced concrete buildings subjected to seismic actions (Kwon and Elnashai, 2006). For the consideration of uncertainties in ground motions, a ground motion set as

representative of earthquake characteristics of the target region is necessary for the fragility analysis. The amount of sufficient number of ground motions is a controversial topic among researchers. It depends on response types of structures (whether mean values or distributions of responses are needed), analysis method accuracy, prediction of maximum response and expected level of inelastic response (Haselton et al., 2012). For this reason, the appropriate number of ground motions is specific for each study. For mid-rise buildings, usually, 10-20 ground motion records are sufficient for the estimation of seismic performance with a sufficient level of accuracy (Shome and Cornell, 1999).

In this study, for the consideration of ground motion uncertainty in the derivation of fragility functions, 25 ground motion pairs are selected from the PEER Strong Motion database (http://peer.berkeley.edu) and they are listed in Table 2.1. They are consistent with the disaggregation results. The selected ground motions are recorded on stiff soil conditions (ZC and ZD soil class in TBEC (2018) within a $(V_s)_{30}$ range between 180-720 m/s). All ground motions have a magnitude (M_w) between 6.0-7.6 and Joyner-Boore distance (J_{BR}) between 15-35 km. They have strike-slip fault types. No more than three records are used per one event. Figure 2.10, Figure 2.11 and Figure 2.12 show the variation of the abovesaid parameters with respect to the geomean value of PGA and PGV of the selected ground motions in log scale. A disperse behavior is observed from three plots, especially the distribution of R_{JB} with respect to PGA and PGV. But both PGA and PGV tend to rise as M_w increases and decrease as $(V_s)_{30}$ increases.

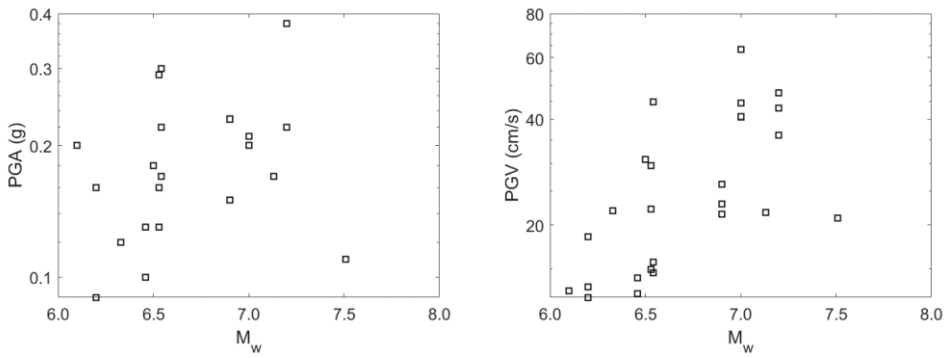

Figure 2.10. Variation of magnitudes with respect to geomean PGV and geomean PGA values for 25 ground motion pairs used in this study.

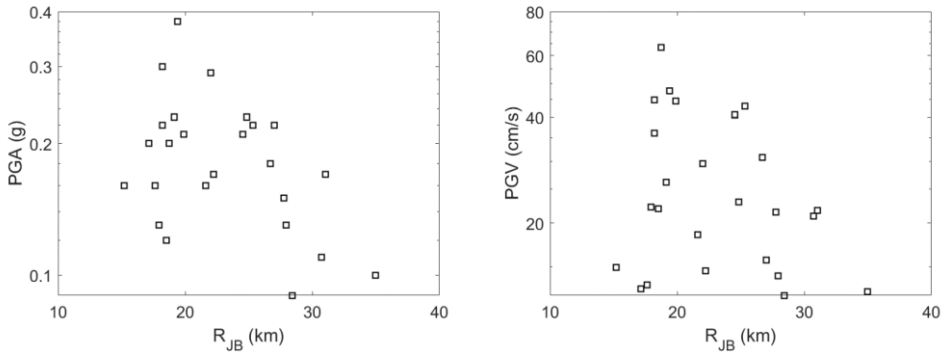

Figure 2.11. Variation of Joyner-Boore distance with respect to geomean PGV and geomean PGA values for 25 ground motion pairs used in this study.

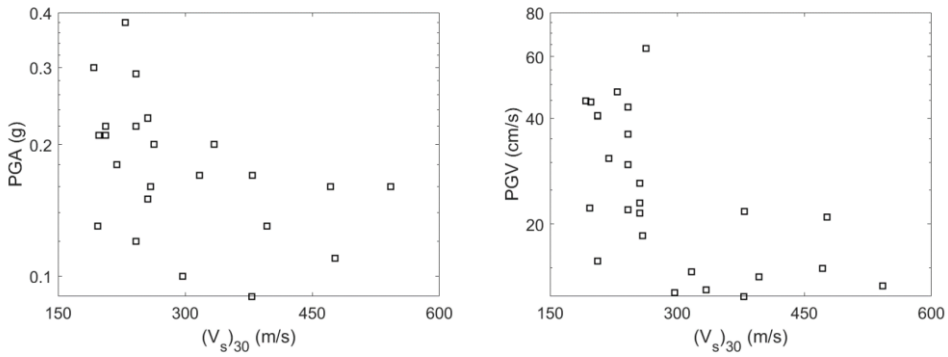

Figure 2.12. Variation of shear wave velocities recorded 30 m below the top of the soil layer with respect to geomean PGV and geomean PGA values for 25 ground motion pairs used in this study.

Table 2.1. Ground motion list used in this study.

Earthquake Name	Year	Station	M_w	R_{JB} (km)	V_{S30} (m/s)	H1-PGA (g)	H2-PGA (g)	H1-PGV (cm/s)	H2-PGV (cm/s)
Victoria_ Mexico	1980	Chihuahua	6.33	18.53	242	0.15	0.10	26.01	18.49
Superstition Hills-02	1987	Plaster City	6.54	22.25	317	0.14	0.20	9.86	21.60
Superstition Hills-02	1987	Calipatria Fire Station	6.54	27.00	206	0.19	0.26	16.43	14.97
Superstition Hills-02	1987	El Centro Imp. Co. Cent	6.54	18.20	192	0.36	0.26	48.07	41.79
Northern Calif-03	1954	Ferndale City Hall	6.50	26.72	219	0.16	0.20	36.07	26.21
Kocaeli_ Turkey	1999	Iznik	7.51	30.73	477	0.09	0.12	17.30	25.26
Kobe_ Japan	1995	Abeno	6.90	24.85	256	0.22	0.23	21.25	24.78
Kobe_ Japan	1995	Shin-Osaka	6.90	19.14	256	0.23	0.23	31.33	21.81
Kobe_ Japan	1995	Yae	6.90	27.77	256	0.16	0.15	21.19	21.74
Joshua Tree_ CA	1992	Thousand Palms Post Office	6.10	17.15	334	0.20	0.20	13.57	12.43
Imperial Valley-06	1979	Cerro Prieto	6.53	15.19	472	0.17	0.16	11.55	19.28
Imperial Valley-06	1979	Delta	6.53	22.03	242	0.24	0.35	26.32	33.00
Imperial Valley-06	1979	El Centro Array #12	6.53	17.94	197	0.14	0.12	21.49	23.00
Hector Mine	1999	Joshua Tree	7.13	31.06	379	0.15	0.19	19.15	24.71
El Mayor-Cucapah_ Mexico	2010	Chihuahua	7.20	18.21	242	0.25	0.20	38.35	34.00
El Mayor-Cucapah_ Mexico	2010	TAMAULIPAS	7.20	25.32	242	0.21	0.23	34.96	52.82
El Mayor-Cucapah_ Mexico	2010	El Centro - Imperial & Ross	7.20	19.39	229	0.38	0.37	47.37	47.62
Darfield_ New Zealand	2010	Christchurch Cathedral College	7.00	19.89	198	0.19	0.23	59.17	33.46
Darfield_ New Zealand	2010	Papanui High School	7.00	18.73	263	0.21	0.18	51.28	78.05
Darfield_ New Zealand	2010	Pages Road Pumping Station	7.00	24.55	206	0.20	0.22	29.38	56.24
Chi-Chi_ Taiwan-04	1999	CHY034	6.20	28.45	379	0.08	0.10	16.45	9.40
Chi-Chi_ Taiwan-04	1999	CHY028	6.20	17.63	543	0.12	0.21	12.58	14.10
Chi-Chi_ Taiwan-04	1999	CHY101	6.20	21.62	259	0.15	0.18	18.85	18.13
Big Bear-01	1992	San Bernardino - E & Hospitality	6.46	34.98	297	0.09	0.10	13.75	11.84
Big Bear-01	1992	Morongo Valley Fire Station	6.46	27.96	396	0.15	0.12	15.97	12.52

2.4.3. Application of Ground Motions to the Structural Models

For fragility analysis, EDPs can be obtained from NRHA by use of ground motion records. Such ground motions should represent all levels of the seismic hazard at the target region. The hazard curves that are specific to İstanbul and determined by use of three abovesaid GMPEs are illustrated in Figure 2.13. In this study, two horizontal components of ground motions are applied to 3-D building models at the same time. For all ground motions, the geomean PGV value is calculated first. Then, the ground motions are scaled such that geomean PGV is equal to 2.5 cm/s. Ground motion pairs are applied to 3-D building models in two orientations by switching the place of two horizontal components in order to get a more robust prediction of EDPs. The scaled ground motions are increased with 1.3 factor for the consideration of directional uncertainty in the perpendicular components of the records. This is a common practice in the application of ground motion pairs to 3-D building models in multiple orientations. To cover all seismic hazard levels, ground motions are increased with 2.5 cm/s intervals of geomean PGV values and NRHA continues until dynamic instability is observed.

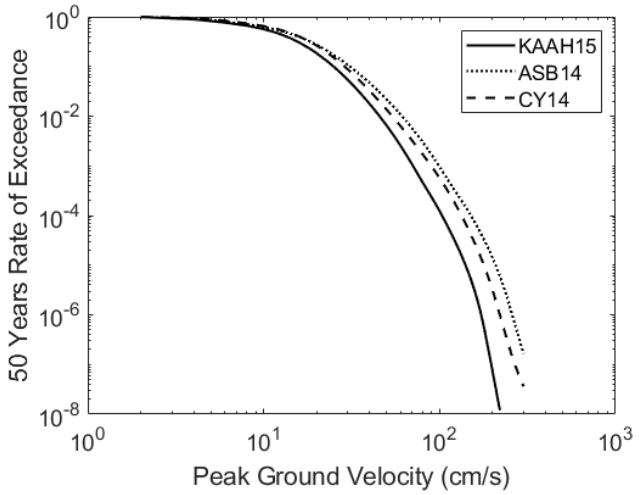

Figure 2.13. Hazard curves for İstanbul.

3. INCREMENTAL DYNAMIC ANALYSIS

3.1. Description of Incremental Dynamic Analysis

The main interest in performance-based earthquake engineering (PBEE) is the correct estimation of structural performance under seismic loads. NRHA is the most realistic way to predict response parameters of the buildings subjected to earthquakes. Incremental dynamic analysis (IDA) (Vamvatsikos and Cornell, 2002), or dynamic pushover (DPO) is a comprehensive computer-intensive analysis method for the estimation of seismic performance of structures. It involves scaling of ground motions to multiple levels of intensity and subjecting structural models to these scaled ground motions in order to generate curves representing relationships between structural responses and ground motion intensities. With the application of IDA, the changes in structural response parameters (from elastic range to the collapse) under increasing ground motion intensity level can be observed and, the differences in structural demands from one record to another can be understood. In addition, dynamic strength and deformation capacity of the structures can be estimated. In order to start IDA, an unscaled acceleration time history is multiplied by monotonically varying scale factors for the consideration of milder or more severe ground motions. Obviously, IMs of the scaled ground motions are proportional to the scale factors. The selected IM should be monotonically scalable. PGA, PGV, and S_a (T_1) are examples of monotonically scalable IMs whereas duration, MMI and moment magnitude are examples of non-scalable ones (Vamvatsikos and Cornell, 2002). A suitable DM like MIDR, maximum compression strain of columns or maximum base shear force is needed for the representation of structural response during NRHA. Based on the above definitions, NRHA is applied to a SDOF or MDOF system with the scaled ground motions. DMs at each IM level are recorded during analyses. At the end, the DM versus IM plot called the IDA curve is generated.

IDA curves are specific for each structural model and ground motion record. The results might be quite dissimilar when different building models or acceleration time histories are used (Vamvatsikos and Cornell, 2002). IDA curves start with a linear elastic branch called elastic stiffness of the IDA curve if the structure is initially linearly elastic.

For MDOF systems, the linear elastic branch may change from one record to another if higher mode effects are not considered. This branch ends up when the first nonlinearity occurs in a structural element of the building. After the linear elastic branch, when the structure experience higher acceleration, the accumulation of the DM increases. As a result, the curve softens and, larger deformations are observed for higher values of the IMs (see Figure 3.1 (a)). On the other hand, when the structure experiences deacceleration, and if it is strong enough to stop the DM accumulation for an instant, a hardening behavior is observed (see Figure 3.1 (b) and (c)). The stiffness of the IDA curves is higher when hardening behavior is observed. The DM accumulation may even be reversed as a result of deacceleration (Vamvatsikos and Cornell, 2002). In addition, a wavy behavior including both softening and hardening behaviors can be observed together in an IDA curve after the linear elastic branch (see Figure 3.1 (c) and (d)). Dynamic instability might be observed when the structural model accumulates the DM at higher rates. That is, when small increments in the IM cause larger deformations that end up with the infinity, a flatline behavior expressing dynamic instability is observed (see Figure 3.1 (a), (b) and (e)).

There might be still a doubt on the hardening behavior of IDA curves that the structure experiences less damage at higher IM levels. This is due to the timing and the pattern of the accelerograms rather than intensity (Vamvatsikos and Cornell, 2002). When the acceleration time history is scaled up, initial weak cycles of the record may become intense enough to cause yielding of the structure. This condition changes the response of the structure under upcoming stronger cycles. The structure may become less responsive to that stronger cycles after yielding. Due to this condition, after dynamic instability is observed, non-collapse situation might be observed at higher IM levels. This is an extreme case of hardening named as the structural resurrection (Vamvatsikos and Cornell, 2002) (see Figure 3.1 (e)).

A single-record IDA cannot display full response ranges of a building under increasing seismic actions (Vamvatsikos and Cornell, 2002). In order to illustrate the complete behavior of a building, IDA is applied to the same structural model using a large suite of suitable earthquake records (20 or more) (FEMA-P58, 2012). Then, results of the IDA are plotted on the same figure displaying the IM versus DM relationships (IDA curve set). While a single-record IDA displays a deterministic behavior, a multi-record IDA

represents a probabilistic characterization due to the record-to-record variability. The results of a suite of records can be summarized by use of mean or 16%, 50% (median) and 84% fractiles of multi-record the IDA curves (Vamvatsikos and Cornell, 2002).

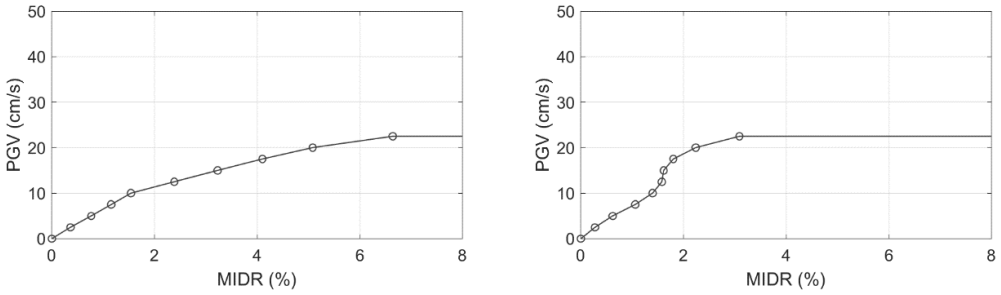

(a) Softening

(b) A bit of hardening

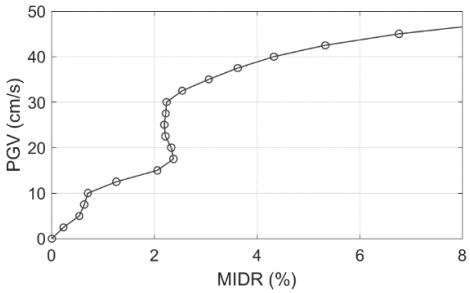

(c) Severe hardening

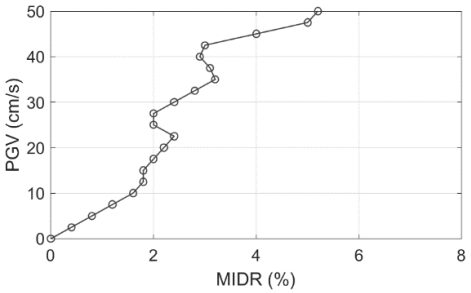

(d) Weaving

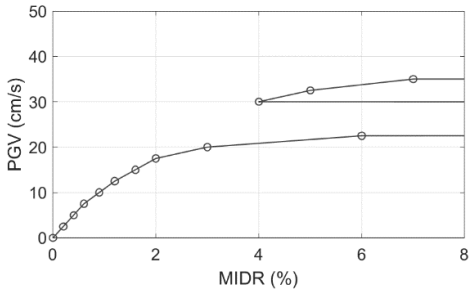

(e) Resurrection

Figure 3.1. Typical behaviors of IDA curves.

IDA curves include necessary information for the assessment of structural performance levels. It is possible to associate limit states in terms of a DM value. When the DM value exceeds a predefined certain limit value, the structure is considered to be in the limit state. This method is called as the DM-based rule (Vamvatsikos and Cornell, 2002).

To illustrate, some relevant codes like FEMA 350 (SAC, 2000a), HAZUS MR4 (NIBS, 2004), ASCE/SEI-41 (2006), SEAOC (1999) and TEC (2007) provide limit states in terms of MIDR. Alternatively, the IM-based rule can be used for the determination of limit states (Vamvatsikos and Cornell, 2002). In this method, signals from the IDA curves are associated with the limit states. To illustrate, yielding of the structure can be considered as the point where first nonlinearity occurs on the IDA curve. Similarly, the global collapse of the structure is related to the DM and IM value where flatline is observed. In addition, the collapse of the building model can be considered as the point where excessively higher DM value is observed at an increment when compared to previous ones. That is, the flattening of the curve is an indicator of dynamic instability. For example, FEMA 350 (SAC, 2000a) associates the collapse value of the DM at the last point on the curve whose tangent slope is equal to 20% of the initial elastic slope (Vamvatsikos and Cornell, 2002). This method is useful if the structural models show collapse behavior with a finite DM output (like 10% MIDR) rather than dynamic instability. Collapse simulation of the structural models is a challenging issue in nonlinear modeling. It highly depends on the capabilities of the computer software used as well as definitions and assumptions in nonlinear modeling. For this reason, using a DM-based rule is advantageous due to its simplicity. For both rules, there might be multiple IM values corresponding to limit values of DM due to the weaving behavior of IDA curves (see Figure 3.1 (c), (d) and (e)). At this point, the lowest IM value can be considered as the limit state point in order to be on the conservative side (Vamvatsikos and Cornell, 2002). In addition, since limit states calculated according to the IM-based rule change curve by curve in multi-record IDA curves, they should be determined for every single curve separately.

3.2. Selection of Intensity Measure and Damage Measure

In PSHA, the severity of the ground motions is generally defined by PGA, PGV, and S_a using an attenuation relationship. With these common ground motion indices, it is more practical to represent future earthquakes (Molas et al., 2004). Effective IM choice is important in PBEE. To illustrate, in an IDA study, smaller dispersion of an IM for a given DM implies that a smaller number of NRHA and a smaller number of ground motion records is needed for the estimation of the median IDA curve (Vamvatsikos and Cornell, 2002). Therefore, in multi-record IDA studies, small dispersion is expected in order to

improve the robustness of response of the buildings. In addition, smaller dispersion increases the legitimacy of using weaker earthquakes to represent stronger ones by a scaling procedure (Vamvatsikos and Cornell, 2002). The effective choice of the IM significantly depends on the structure type. For example, first-mode dominant structures (like low-rise or mid-rise buildings) are sensitive to S_a (T_1). When higher mode contributions are important for a structure type (like high-rise buildings), the correlation between damage and spectral quantities is week. For short period structures, i.e., stiff structures (like low-rise buildings), PGA correlates well with the damage. For the structures in the intermediate period range (like mid-rise buildings), PGV is a better damage indicator. In addition, for the evaluation of large building stocks, structural period independent IMs like PGA and PGV are mostly preferred. From past studies, it is observed that PGV correlates well with inelastic displacement demands (Akkar at el., 2005). It is a more reliable intensity indicator of ground motions (Sucuoğlu and Erberik, 1998). PGV reflects the deformation demands of buildings better when they are in the inelastic range (Akkar and Özen, 2005). Therefore, in this study, PGV is selected as the IM.

3.3. Evaluation of IDA Curves

IDA is applied to the building models in order to determine structural demands under earthquake loads by use of 3.0 version of OpenSees (UC Berkeley, 2019) software. A total number of 9535 3-D bidirectional NRHA is performed on 16 no-code mid-rise RC MRF building models using 25 incrementally scaled real ground motion pairs. Through IDA, PGV of the ground motions are monotonically increased with 2.5 cm/s intervals (see Chapter 2.4.3). Analyses are stopped when the first numerical non-convergence is observed. Interstory drift ratio, top displacement and base shear of the building models, as well as chord rotation, concrete strain, reinforcement strain and internal force of the structural members are recorded at each NRHA for the evaluation of seismic performance and the generation of fragility curves that are discussed in Chapter 4. Interstory drift ratios and lateral deformations are mostly used DMs in earthquake response analysis of the structures. MIDR is a suitable selection for the evaluation of structural damage (FEMA-P58, 2012). Therefore, in this study, multi-record IDA curves are plotted in terms of MIDR against PGV including 16%, 50% (median) and 84% fractiles for each building (see Figure 3.2 and Figure 3.3).

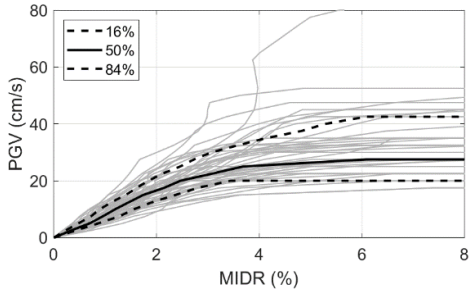

(a) Model01 (Type-1)

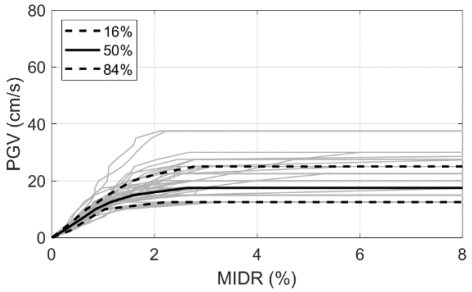

(b) Model02 (Type-2)

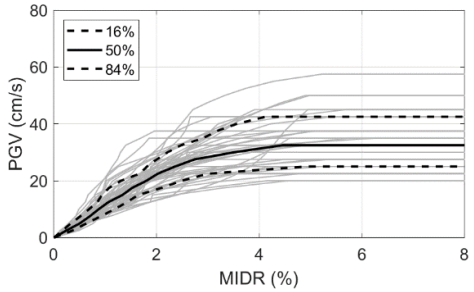

(c) Model03 (Type-1)

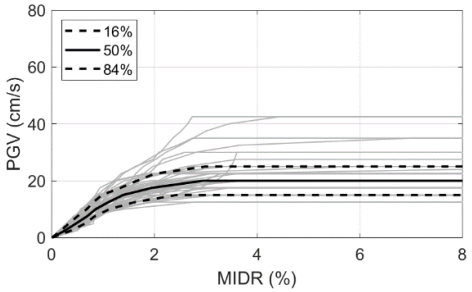

(d) Model04 (Type-2)

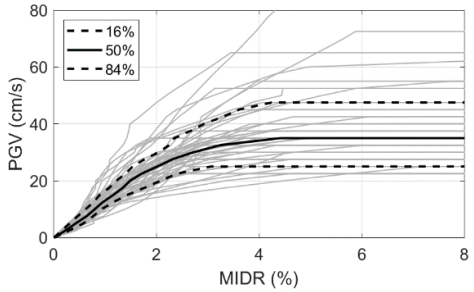

(e) Model05 (Type-1)

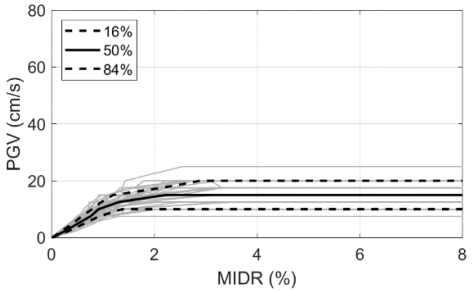

(f) Model06 (Type-2)

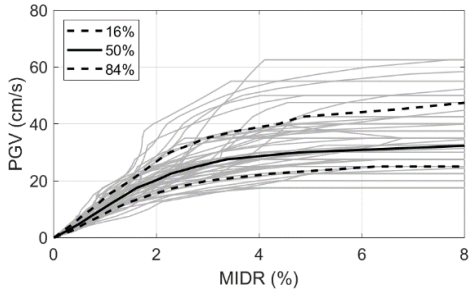

(g) Model07 (Type-1)

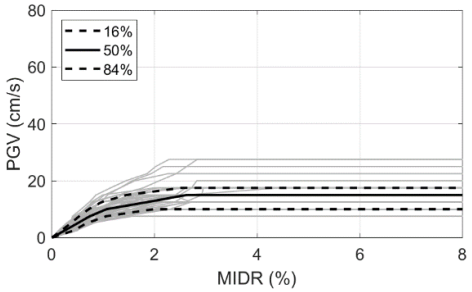

(h) Model08 (Type-2)

Figure 3.2. MIDR response of 16 building models as a result of IDA. cont.

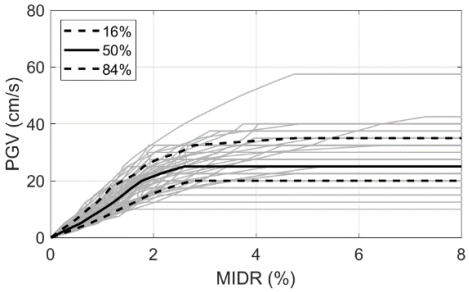

(i) Model09 (Type-1)

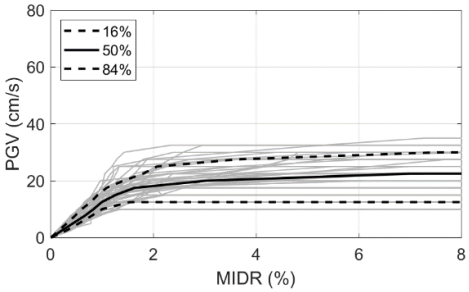

(j) Model10 (Type-2)

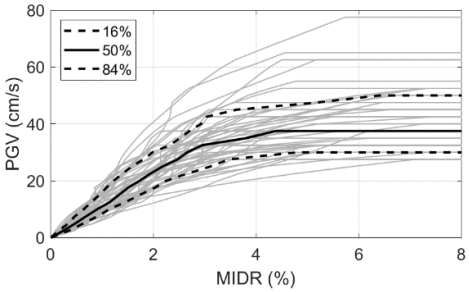

(k) Model11 (Type-1)

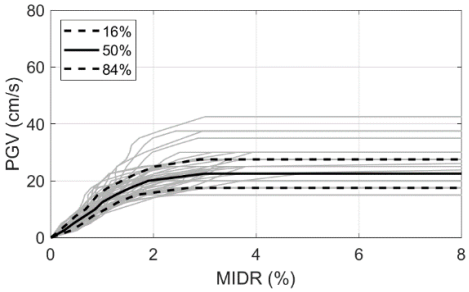

(l) Model12 (Type-2)

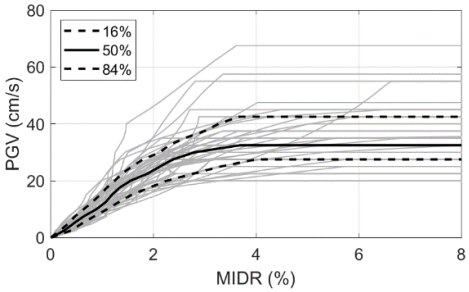

(m) Model13 (Type-1)

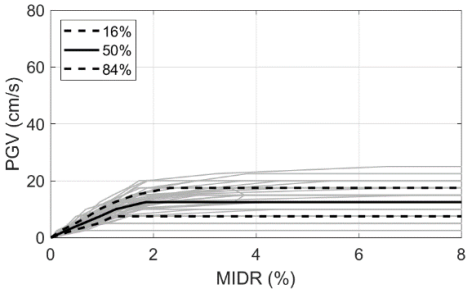

(n) Model14 (Type-2)

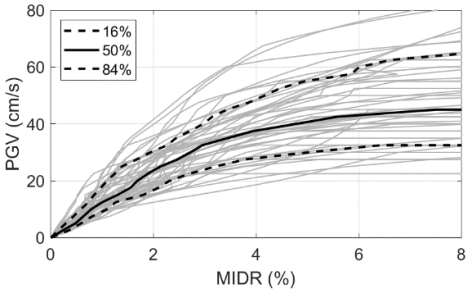

(o) Model15 (Type-1)

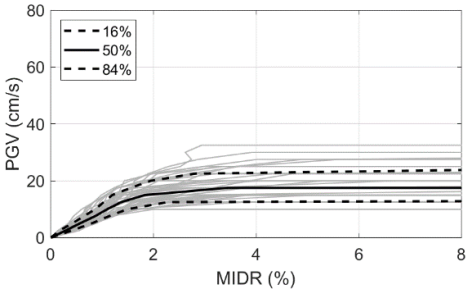

(p) Model16 (Type-2)

Figure 3.3. MIDR response of 16 building models as a result of IDA.

Multi-record IDA curves guide researchers to understand the response of buildings under the random feature of ground motion excitations. The importance of ground motion variability can be seen from the IDA curve sets (see Figure 3.2 and Figure 3.3). All IDA curves start with the initial linear branch, continue with softening and/or hardening behavior and finally end up with global instability indicating structural collapse. For each building, the dispersion, which can be defined as the difference between maximum and minimum values of the IM for a given DM, is less for the initial branch. The dispersion is higher after the initial branch due to the timing and the pattern of the acceleration time histories. In addition, it is observed that the dispersion is higher for the Type-1 buildings since they have the capability of experiencing higher IM levels when compared to the Type-2 buildings.

In order to understand the variety of response parameters of different structural models, the median IDA curves of 16 building models are plotted on the same graph (see Figure 3.4). Although initial branches of the median IDA curves are so close to each other, after this branch, considerable differences are observed in terms of response statistics. As expected, the Type-2 buildings having unconfinement mechanism and poorer reinforcement detailing have less deformation capacity. The dynamic instability is observed at lower IM levels for the Type-2 buildings.

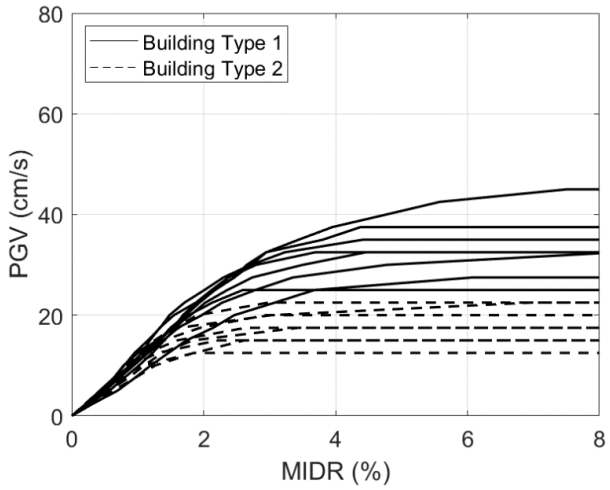

Figure 3.4. Median IDA curves of 16 building models.

3.4. Comparison of IM Correlations with Calculated Damage

Correlation is a statistical term that investigates the degree of relationship (usually linear) between two or more variables. The correlation coefficient (R) is a numerical value changing between zero and one. It indicates the dispersion of the data. A value of the correlation coefficient close to one implies well correlation and less dispersion. Correlation of ground motion indices and engineering demand parameters are important in PBEE as mentioned before. Therefore, in this study, correlation coefficients are calculated between IMs and DM based on results of NRHA in the form of IDA (Vamvatsikos and Cornell, 2002). IMs are considered as PGA, PGV, and S_a (T_1) since they are mostly used IMs in PBEE. DM is considered as MIDR since it is a global response parameter that represents the structural damage well. At the end, the IM that correlates best with the given DM is determined.

A linear relationship between logarithms of two data sets usually provides an acceptable prediction of the mean value of the DM over a range of IM (Baker, 2007). Therefore, a linear relationship is assumed between natural logarithms of the PGA-MIDR, PGV-MIDR, and S_a (T_1)-MIDR pairs. As mentioned before, IDA is applied to the building models with monotonic increments of geomean PGV values of the bidirectional ground motions. At each analysis, using scale factors, geomean PGA and geomean S_a (T_1) values of the ground motions are calculated. Since 3-D models are used in this study, T_1 is calculated using the arithmetic mean of the periods in two principle directions of each building. IMs are plotted with corresponding MIDR values in the log-scaled scatter diagrams. Linear regression analysis is carried out using the natural logarithms of the pairs. Trend lines are fitted through the scatter diagrams and, correlation coefficients of the natural logarithms of the pairs (or the coefficient of determination, R^2) are calculated (see Figure 3.5, Figure 3.6 and Figure 3.7). It is 0.77, 0.91 and 0.80 for PGA-MIDR, PGV-MIDR and S_a (T_1)-MIDR pairs, respectively. The results show that MIDR values for a given PGA, PGV or S_a (T_1) value display a disperse behavior due to the variety in structural models and ground motion records. PGV has smaller dispersion and it correlates better with observed structural damage when compared to PGA and S_a (T_1) for subject buildings.

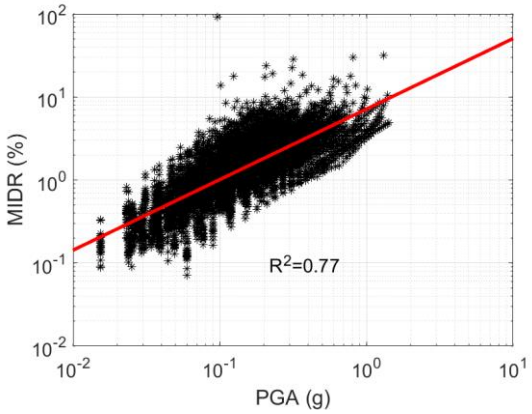

Figure 3.5. PGA vs. MIDR relationships as a result of 9535 NRHA.

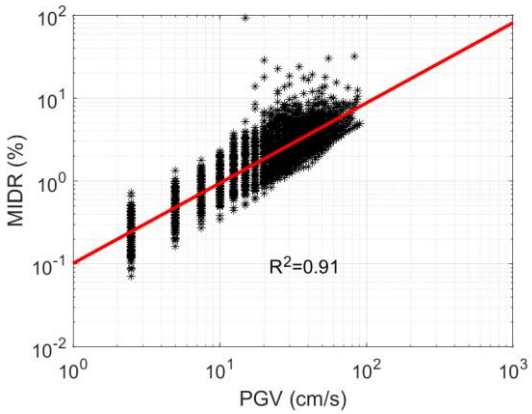

Figure 3.6. PGV vs. MIDR relationships as a result of 9535 NRHA.

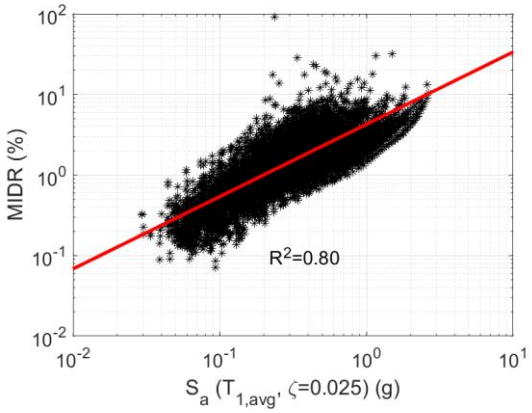

Figure 3.7. S_a ($T_{1,avg}$)) vs. MIDR relationships as a result of 9535 NRHA.

3.5. Comparison of IDA and Pushover Curves

In an IDA study, since EDPs are related to the IMs, IDA curves represent EDP-IM relationships. However, pushover analysis provides capacity curves illustrating a displacement demand against the total base shear of the building. This section compares the results obtained from IDA and pushover analysis. IDA and pushover curves of 16 RC building models are plotted in previous sections. Comparison is done in the form of capacity curves indicating η-MIDR relationships. Therefore, during each single record IDA and at each increment, MIDR and maximum value of η through time steps are calculated in both principal directions for each building model. At the end, dynamic capacity curves representing the MIDR response as a function of maximum η instead of an IM (PGV in this case) are plotted. Since building models are subjected to 25 ground motion pairs in two orientations, a large variability is observed between the results of each single record IDA. Therefore, the results are summarized using the median values of MIDR and maximum η for each building model. It should be emphasized that maximum η is also an EDP like MIDR (Fragiadakis and Vamvatsikos, 2011). Therefore, interrelation of 2 EDPs is monitored using IDA results. To summarize, IDA curves are converted to force-displacement plots so that the results obtained from IDA and pushover analyses are compared at a global level. Capacity curves displaying relationships between MIDR and maximum values of η obtained from both analyses are illustrated in Figure 3.8, Figure 3.9, Figure 3.10 and Figure 3.11. The median IDA curve is considered to be a better indicator when compared to the single record IDA curves since it summarizes 50 single record IDA curves. That is, it considers the variety in time and pattern of the 25 ground motion pairs. The results show that IDA curves generally follow the pushover curves. A good correlation is observed between pushover and median IDA curves of building models, especially curves of Model03 and Model05 in x-direction. But for most of the cases, building base shear capacity is higher in median IDA curves. The difference is high for y-direction of Model05 and Model11. Obviously, these differences come from the theories behind two analysis types. Pushover analysis does not consider the energy and the frequency content as well as time and pattern of seismic actions. Therefore, the yielding pattern of the structural members is different in both analysis types. As a result, pushover analysis underestimates the building capacities of subject buildings.

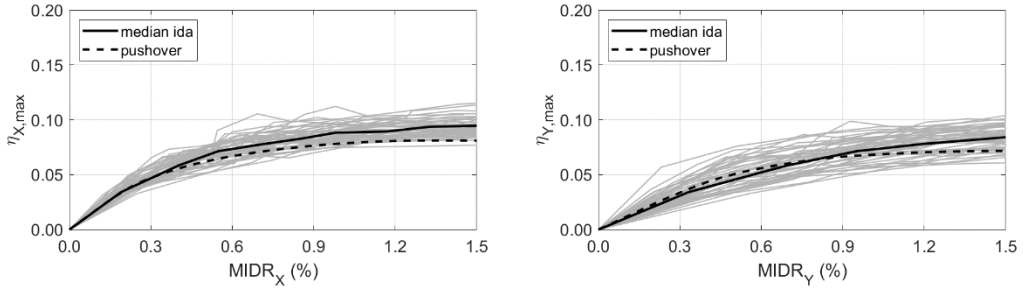

(a) Model01 (Type-1)

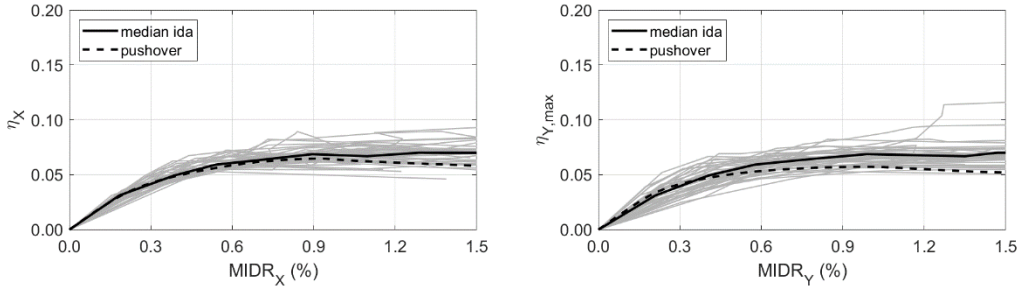

(b) Model02 (Type-2)

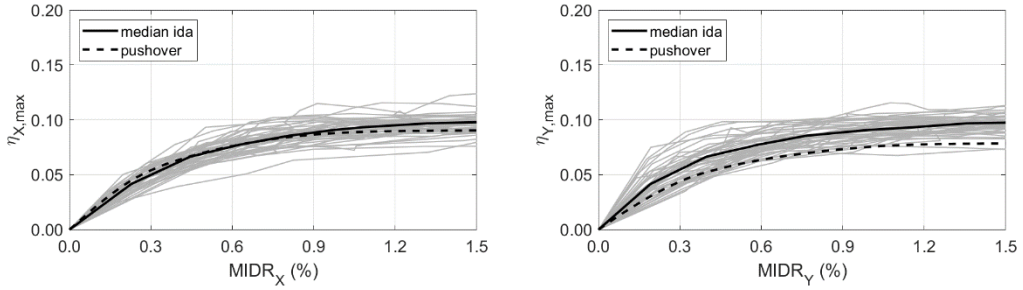

(c) Model03 (Type-1)

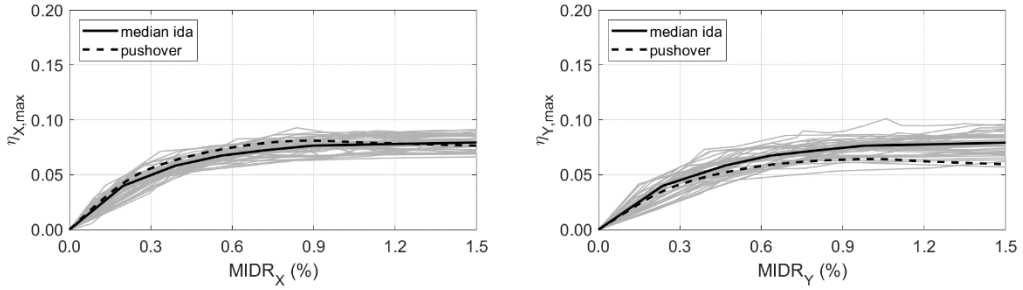

(d) Model04 (Type-2)

Figure 3.8. Comparison of IDA and pushover curves of 16 building models. cont.

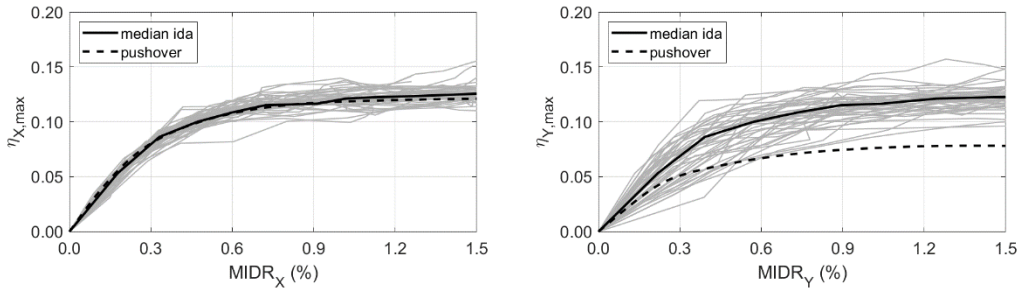

(e) Model05 (Type-1)

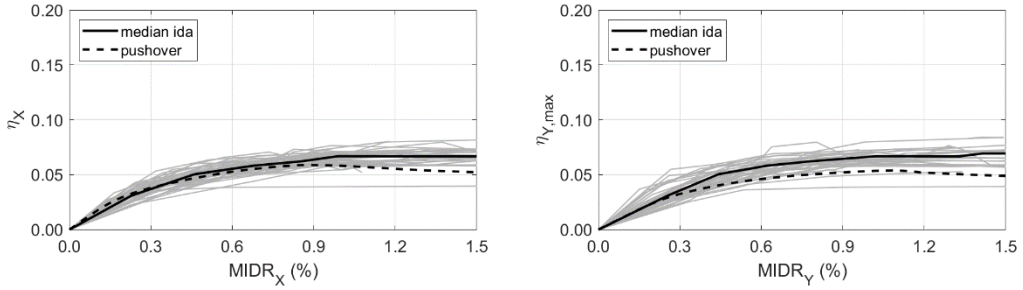

(f) Model06 (Type-2)

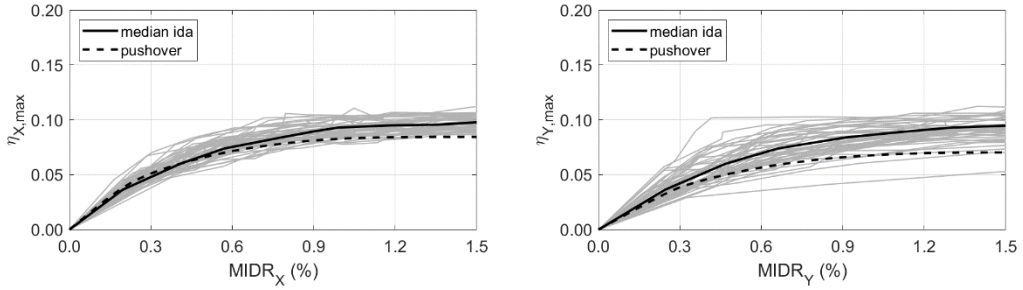

(g) Model07 (Type-1)

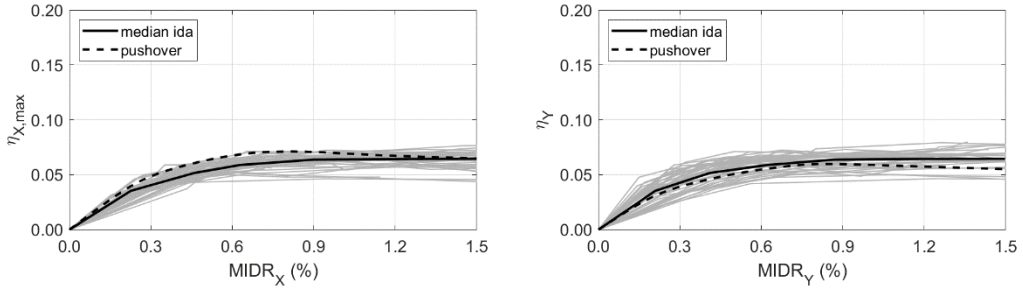

(h) Model08 (Type-2)

Figure 3.9. Comparison of IDA and pushover curves of 16 building models. cont.

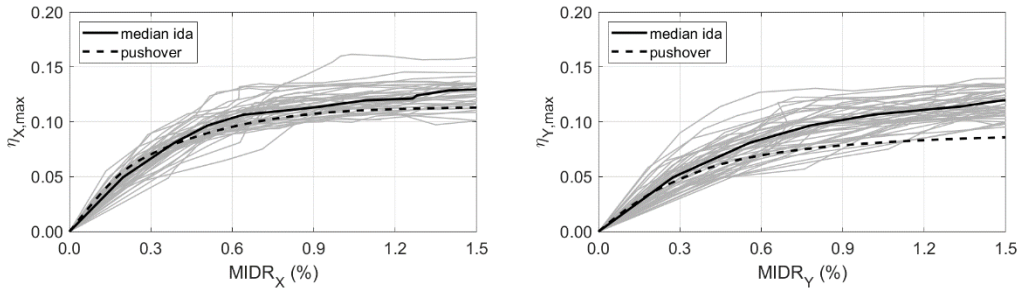

(i) Model09 (Type-1)

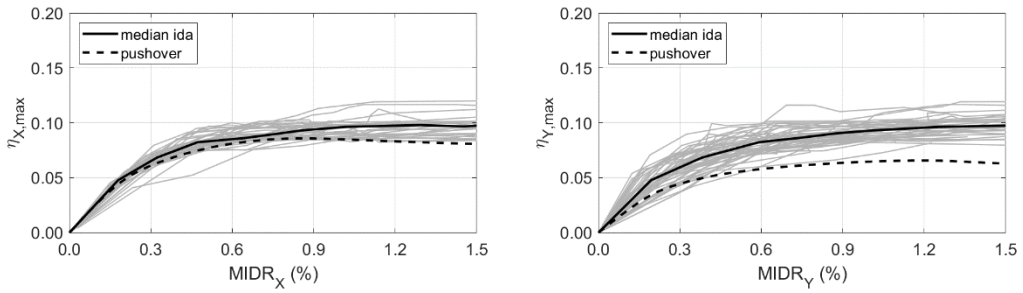

(j) Model10 (Type-2)

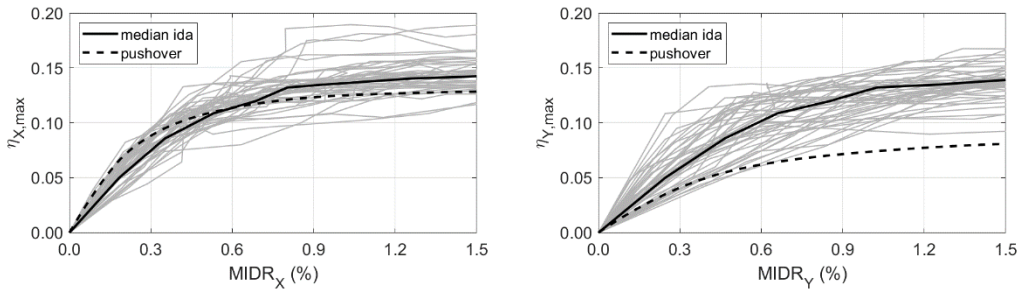

(k) Model11 (Type-1)

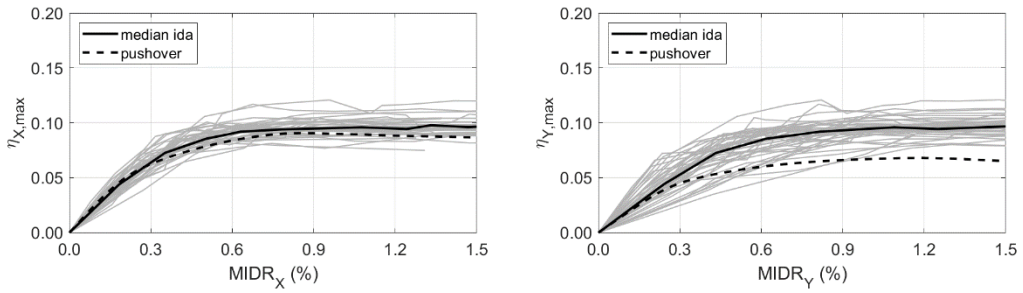

(l) Model12 (Type-2)

Figure 3.10. Comparison of IDA and pushover curves of 16 building models. cont.

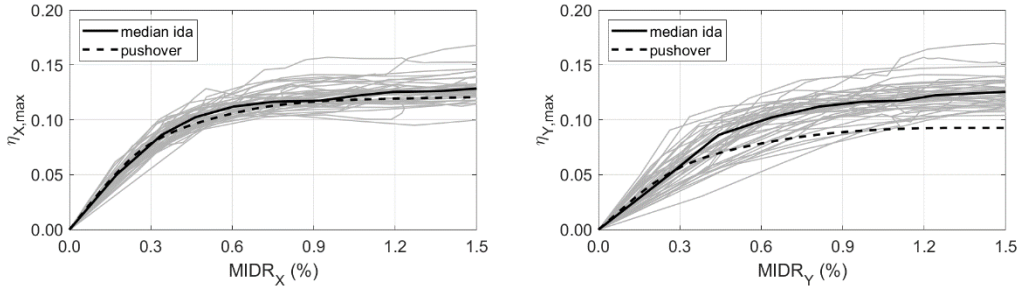

(m) Model13 (Type-1)

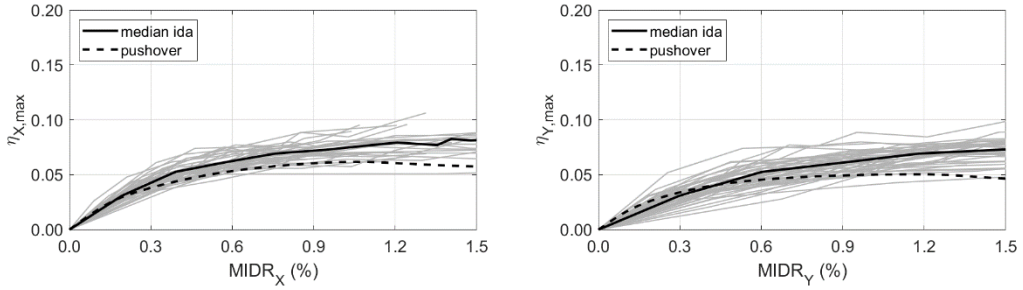

(n) Model14 (Type-2)

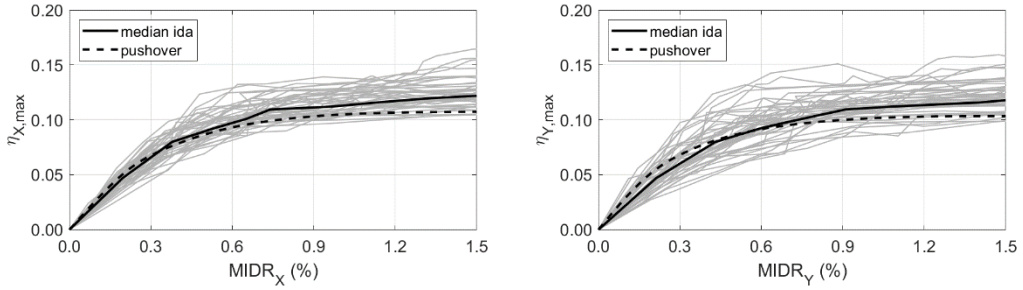

(o) Model15 (Type-1)

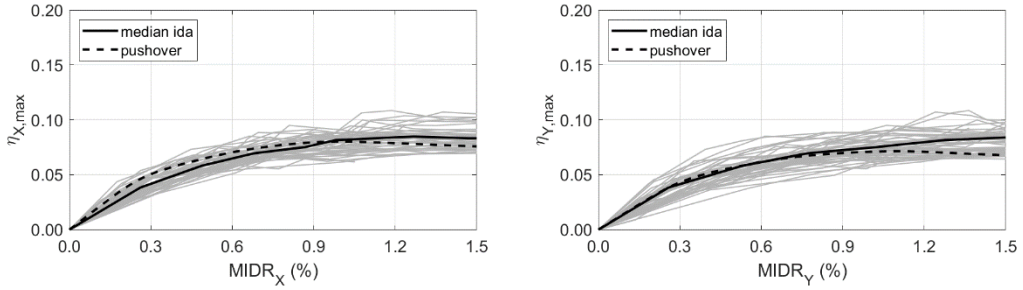

(p) Model16 (Type-2)

Figure 3.11. Comparison of IDA and pushover curves of 16 building models.

4. FRAGILITY ASSESSMENT

4.1. Attainment of Limit States

Comprehensive and realistic determination of limit states and therefore, identification of performance levels is one of the substantial steps in fragility curve derivation because they affect resulting fragility functions directly (Erberik and Elnashai, 2004). Simply, a limit state is a numerical value in terms of forces or deformations. It is the last point where the system cannot satisfy a performance level. Local or global limit state definitions can be made. Maximum global drift ratio and MIDR are the most commonly used parameters in global limit state definitions. Local limit states can be defined in terms of rotations and strains for structural members. In NRHA, the cyclic behavior of the structural members highly affects the overall response of the building. Therefore, limit state definitions of structural members become highly important for fragility analysis. They can be used for the generation of building component fragility curves. However, for fragility assessment of the buildings, the local performance levels must be converted to the global performance levels of the buildings.

Immediate occupancy, life safety, and collapse prevention are mostly used limit state definitions in the literature. FEMA-356 (2000) defines these limit states. They are summarized below:

- IO (Immediate Occupancy): Very limited damage is observed on the structure after the earthquake. The vertical and lateral load carrying system is almost the same as the pre-earthquake situation.
- LS (Life Safety): Significant damage is observed on the structure after the earthquake. There is some margin against structural collapse (partial or total). Although some structural members are severely damaged, this situation does not lead to hazards of large falling debris (inside and outside of the structure). The risk of life-threating injury as a result of damage to the structure is low.

- CP (Collapse Prevention): The structure is near the situation of total or partial collapse. The lateral load-carrying system is severely damaged. Injury risk as a result of falling debris may occur. The structure is not safe for reoccupation.

Similar limit state definitions are provided in the TBEC (2018) and Eurocode 8 (2005). In this study, the limit states are determined using structural member performances. Column and beam performances are determined from TBEC (2018) and Eurocode 8 (2005) separately. Then, the global performances of the buildings are determined by the regulations of TBEC (2018).

4.1.1. Performance of Structural Members using TBEC (2018)

TBEC (2018) provides three limit states as Limited Damage (LD), Controlled Damage (CD) and Collapse Prevention (CP) in terms of concrete and reinforcement strain for structural members modeled with distributed plasticity. Concrete strain limits are expressed as:

$$\varepsilon_c^{CP} = 0.0035 + 0.04\sqrt{\omega_{we}} \leq 0.018 \tag{4.1}$$

$$\varepsilon_c^{CD} = 0.75\varepsilon_c^{CP} \tag{4.2}$$

$$\varepsilon_s^{LD} = 0.0025 \tag{4.3}$$

where

$$\omega_{we} = \alpha\rho_{sh,min}\frac{f_{ywe}}{f_c} = \left(1 - \frac{\sum a_i^2}{6b_0h_0}\right)\left(1 - \frac{s}{2b_0}\right)\left(1 - \frac{s}{2h_0}\right)\rho_{sh,min}\frac{f_{ywe}}{f_c} \tag{4.4}$$

The first term in Equation (4.1) represents the contribution of unconfined concrete. The second term represents the contribution of the confinement mechanism where ω_{we} is the mechanical reinforcement ratio of effective confinement and α is the confinement effectiveness factor. It depends on the spacing of longitudinal reinforcements (a_i), core dimensions (b_0, h_0), stirrup spacing (s), ratio of transverse steel (ρ_{sh}) as well as concrete

compression strength (f_c) and transverse reinforcement yield strength (f_{ywe}). Obviously, as confinement quality increases (e.g. when lower stirrup spacing or higher transverse steel ratio is used), the CP limit gets higher values, i.e., the LS limit increases. Similarly, reinforcement strain limits are expressed as:

$$\varepsilon_s^{CP} = 0.4\varepsilon_{su} \tag{4.5}$$

$$\varepsilon_s^{CD} = 0.75\varepsilon_s^{CP} \tag{4.6}$$

$$\varepsilon_s^{LD} = 0.0075 \tag{4.7}$$

In Equation (4.5), ε_{su} is the ultimate strength of longitudinal reinforcement. For the members with smooth longitudinal reinforcement bars, i.e., the bars are not ribbed, strain demand of reinforcement is multiplied with 1.5 (TBEC, 2018). In this study, since the subject buildings are no-code buildings that are constructed before 1980, reinforcement bars are accepted to be smooth and reinforcement demand is increased. Using the above equations, strain limits for column and beams are determined and, they are illustrated in Table 4.1. Confined concrete limits are used for Type-1 buildings and unconfined concrete limits are used for Type-2 buildings. When one of the reinforcement or concrete fibers exceeds its limit, then the member is accepted to exceed the limit.

Table 4.1. Strain limits of structural members calculated using TBEC (2018).

Material	IO	LS	CP
Column Confined Concrete	0.0025	0.0097	0.0130
Beam Confined Concrete	0.0025	0.0036	0.0048
Unconfined Concrete	0.0025	0.0026	0.0035
Reinforcement	0.0075	0.0360	0.0480

4.1.2. Performance of Structural Members using Eurocode 8 (2005)

Eurocode 8 (2005) provides three limit states as Damage Limitation (DL), Significant Damage (SD) and Near Collapse (NC) in terms of chord rotations. They are expressed as:

$$\theta^{NC} = \theta_{um} = \frac{1}{\gamma_{el}} 0.016(0.3^{\nu}) \left[\frac{\max(0.01;\omega')}{\max(0.01;\omega)} f_c\right]^{0.225} \left(\frac{L_v}{h}\right)^{0.35} 25^{\left(\alpha\rho_{sx}\frac{f_{yw}}{f_c}\right)} (1.25^{100\rho_d}) \quad (4.8)$$

$$\theta^{SD} = 0.75\theta^{NC} \quad (4.9)$$

$$\theta^{DL} = \theta_y = \phi_y \frac{L_v + a_v z}{3} + 0.00135\left(1 + 1.5\frac{h}{L_v}\right) + \frac{\varepsilon_y}{d-d'}\frac{d_b f_y}{6\sqrt{f_c}} \quad (4.10)$$

The terms in the above formulations are given below:

γ_{el}: 1.5 for primary seismic elements (like columns, walls or main beams)
v: Ratio of compression force and the area of the compression zone
ω, ω': Tension and compression reinforcement ratio, respectively
L_v: Shear span (simply half of the span for columns and beams)
h: Cross-section depth
α: Confinement effectiveness factor (the same with TBEC (2018))
ρ_s: Transverse reinforcement ratio in the direction of loading
f_c: Concrete compression strength
f_y: Longitudinal reinforcement yield strength
f_{yw}: Transverse reinforcement yield strength
ρ_d: Ratio of diagonal reinforcement
ϕ_y: Yield curvature at section end
ε_y: Yield strain of longitudinal reinforcement
d_b: Tension reinforcement diameter (mean)
d, d': Tension and compression reinforcement depth, respectively
z: d-d' for beam and columns

a_v: 1 if shear cracking is expected before flexural yielding (i.e., if the yield moment is higher than the product of shear span and shear resistance of the section without reinforcement), 0 otherwise

For the members detailed without earthquake resistance, the limits are multiplied with 0.825 (Eurocode 8, 2005). In addition, for the members with smooth longitudinal reinforcement bars, the ultimate chord rotation capacity or chord rotation limit of NC is multiplied with 0.575 (Eurocode 8, 2005). In this study, reinforcement bars are accepted to be smooth. Similarly, the structural members are not detailed considering earthquake resistance. Therefore, abovesaid reductions are performed while determining the limit states. Based on the above formulations, the chord rotation limits of every single structural member are determined separately and, they are used to determine the DS of structural members. The mean and standard deviation values of chord rotation limits of columns and beams for Type-1 and Type-2 buildings are illustrated in Table 4.2. The variation of column chord rotation limits comes from member length and axial load as well as different dimensions of columns in both principal directions since the limits are calculated in both principal directions separately. But, the variation of beam chord rotation limits comes only from member length.

Table 4.2. Mean and standard deviation of chord rotation limits (10^{-4} rad) calculated using Eurocode 8 (2005).

Section	Mean			Standard Deviation		
	IO	LS	CP	IO	LS	CP
Type-1 Building Column	0.748	1.868	2.491	0.079	0.157	0.209
Type-1 Building Beam	1.069	1.828	2.438	0.203	0.156	0.208
Type-2 Building Column	0.767	1.469	1.958	0.106	0.147	0.196
Type-2 Building Beam	1.007	1.677	2.236	0.180	0.142	0.186

When compared to strain limits, formulations of rotation limits have a lot of ingredients like member length, the direction of loading, compression force on the member and even the dimension of longitudinal reinforcement. For a cross-section, when limit states are determined in terms of strains, there is only one value for each limit state

definition. That is, strain limits depend only on the cross-section. Therefore, the determination of limit states in terms of strains is more practical.

Note that the difference in TBEC (2018) and Eurocode 8 (2005) may lead to discrepancies in damage state limits if one uses plastic rotation as the common damage state limit. This is explained by a simple example by assuming a fictitious beam having cross-sectional dimensions of 20/50 cm and total span length of 5 m. If TBEC (2018) provisions are followed, reinforcement strain limits for IO, LS and CP are calculated as 0.0050, 0.0240 and 0.0320, respectively. Corresponding total curvature values are calculated as 0.019, 0.058 and 0.077 1/m, respectively under no axial load subjected to the beam. This leads to plastic curvature values of 0.015, 0.054 and 0.073 1/m for IO, LS and CP when specific section analysis results in a yield curvature value of 0.004 1/m. TBEC (2018) specifies plastic hinge length as 50% of the cross-section height (0.25 m for fictious beam). Therefore, the limit plastic rotation values for this fictious beam are calculated as 0.0038, 0.0135 and 0.0183 for IO, LS and CP, respectively. If Eurocode 8 (2005) provisions are followed, one can calculate the chord rotation limits for IO, LS and CP as 0.0054, 0.0242 and 0.0322, respectively. The Eurocode 8 provisions assume chord rotation of IO as the yield rotation. Therefore, the plastic rotation limits of IO, LS and CP are 0.0, 0.0188 and 0.0268, respectively for Eurocode 8 (2005) for this fictious beam. This simple example suggests that the damage limit states provided by TBEC (2018) and Eurocode 8 (2005) will not fully agree with each other and, fragilities presented in the following section should be evaluated under this limited remark.

4.1.3. Global Performance of Buildings

IO, LS and CP performance levels of the subject buildings are determined by the regulations of TBEC (2018) by use of strain and chord rotation limits separately. The code provides global limit states of the buildings (see Figure 4.1) based on the percentage of columns and beams at each local performance level as well as the percentage contribution of column shear forces to the story shear forces. The three performance levels are described as follows:

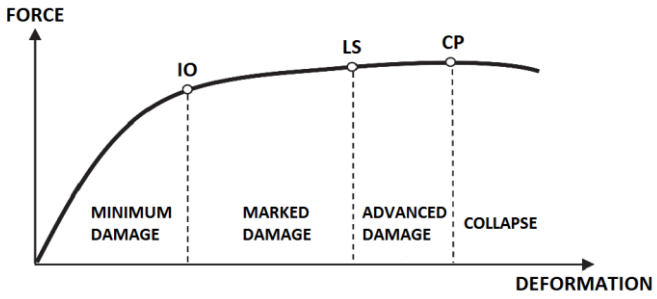

Figure 4.1. Global performance levels of buildings (TBEC, 2018).

IO Performance Level:

- All the columns are in the minimum damage region.
- 20% of the beams can be in the marked damage region. Other beams are in the minimum damage region.
- No brittle shear failure is allowed for columns and beams.

LS Performance Level:

- All the columns are in the minimum damage, marked damage or advanced damage region. But the sum of shear forces of the columns in the advanced damage region is less than 20% of the story shear force. In addition, the sum of shear forces of the columns whose top and bottom regions are in the marked damage or advance damage region is less than 30% of the story shear force.
- 35% of the beams can be in the advanced damage region. Other beams are in the minimum damage or marked damage region.
- No brittle shear failure is allowed for columns and beams.

CP Performance Level:

- All the columns are in the minimum damage, marked damage or advanced damage region. But the sum of shear forces of the columns whose top and

bottom regions are in the marked damage or advance damage region is less than 30% of the story shear force.

- 20% of the beams can be in the collapse region. Other beams are in the minimum damage, marked damage or advanced damage regions.
- Brittle shear failure can only be observed at the beams in the collapse region.

Maximum element responses through time steps of each NRHA are considered for the determination of member performance level (i.e., the maximum value of concrete strain, reinforcement strain, chord rotation, and shear force). The shear force contribution of each column to the story shear force is calculated at each time step of NRHA. The mean value of shear force contribution of each column through time steps is used for performance assessment. When the above three performance levels are not satisfied, the building is in the collapse region. Shear limits of columns and beams are determined with the guidelines of given two codes. Note that brittle shear failure of columns is not allowed for three abovesaid performance levels. In order to avoid useless runs during the IDA, the shear limit of the columns is introduced into OpenSees (UC Berkeley, 2019) software and analyses are stopped when a column reaches its shear capacity. But shear failure of the beams is allowed for the CP performance level if the beam is already in the collapse region because of exceeding the CP limit of strain or chord rotation. For this reason, the shear failure of beams is post-proceed.

4.2. Generation of Analytical Fragility Curves

A statistical procedure proposed by Baker (2011) is followed in order to fit parameters of fragility functions using NRHA results. As mentioned previously, in this study, NRHA of 16 building models is performed in the form of IDA (Vamvatsikos and Cornell, 2002) by use of 25 ground motion pairs at different intensity levels. PGV is selected as IM and during IDA, the intensity of ground motions is increased with 2.5 cm/s intervals of PGV. At each NRHA, DS (performance levels) of the buildings (IO, LS, and CP in this case) is determined. The probability of exceeding a DS at a given PGV level, x, is estimated with the fraction of ground motion records. Then, a lognormal cumulative distribution function (ϕ) is assumed for the continuous estimation of the exceedance probability of each DS as a function of PGV. The proposed equation is given below:

$$P(DS|PGV = x) = \phi\left(\frac{lnx - \mu}{\beta}\right) \tag{4.11}$$

where P(DS|PGV=x) is the exceedance probability of a DS at a given ground motion intensity level (PGV=x), ϕ is a normal cumulative distribution function, μ is the mean of ln(PGV) and β is the standard deviation of ln(PGV) or dispersion of PGV. Note that e^{μ} is the mean of PGV here.

μ and β are estimated using the maximum likelihood estimation (MLE) method (Baker, 2011). For a given IM level, the probability of observing z_j exceedance out of n_j ground motion records with PGV=x_j is given by a binomial distribution as

$$P(z_j \; exceedance \; in \; n_j \; ground \; motions) \; = \binom{n_j}{z_j} p_j^{z_j} (1 - p_j)^{n_j - z_j} \tag{4.12}$$

where p_j is the probability of ground motions with PGV=x_j to exceed a DS for a given structure that is previously defined as P(DS|PGV=x_j) in Equation (4.11). The MLE approach provides the highest probability of observing the exceedance. For multiple PGV levels, the likelihood function that is the product of binomial probabilities at each PGV level is expressed as

$$Likelihood = \prod_{j=1}^{m} \binom{n_j}{z_j} p_j^{z_j} (1 - p_j)^{n_j - z_j} \tag{4.13}$$

where m is the number of PGV levels and Π is a product over all PGV=x_j levels which gives the final probability. The estimations of fragility parameters ($\hat{\mu}$ and $\hat{\beta}$) that maximizes the likelihood are selected for the generation of fragility curves using Equation (4.14).

$$\{\hat{\mu}, \hat{\beta}\} = max_{\mu,\beta} \prod_{j=1}^{m} \binom{n_j}{z_j} p_j^{z_j} (1 - p_j)^{n_j - z_j} \tag{4.14}$$

An example of the fragility curve generated using the MLE method (Baker, 2011) is shown in Figure 4.2 that illustrates the probability of exceedance of a DS as a function of IM (PGV). In this case, there are 50 ground motions. At each IM, NRHA is carried out and exceedance probabilities are calculated. The results are illustrated in Table 4.3. Then, using the abovesaid statistical procedure, mean (μ) and standard deviation (β) values that maximize the likelihood are selected for the continuous estimation of exceedance probability (μ is 2.823 and β is 0.225 in this case). The observed fractions and lognormal fit are illustrated in Figure 4.2.

Table 4.3. Example calculation of exceedance probability of a given DS for discrete levels of IM (PGV).

PGV (cm/s)	2.5	5.0	7.5	10.0	12.5	15.0	17.5	20.0	22.5	25.0	27.5	30.0	32.5	35.0	37.5	40.0
# of exceedance	0	0	0	0	5	18	27	39	44	47	50	50	50	50	50	50
# of analysis	50	50	50	50	50	50	50	50	50	50	50	50	50	50	50	50
Probability	0.00	0.00	0.00	0.00	0.10	0.36	0.54	0.78	0.88	0.94	1.00	1.00	1.00	1.00	1.00	1.00

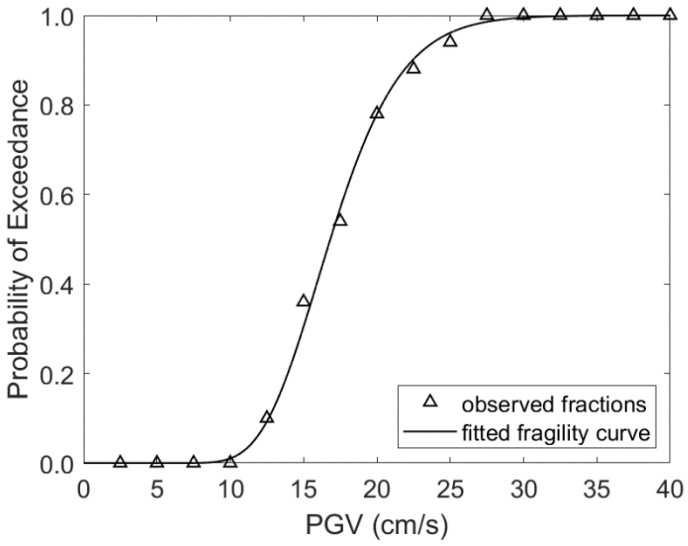

Figure 4.2. Example fragility curve.

4.3. Evaluation of Fragility Curves

PGV based fragility curves of 16 no-code mid-rise RC MRF building models are generated by use of strain and chord rotation limits of structural members, separately. IDA results are post-proceed in order to fit a two-parameter lognormal curve to the exceedance probability of IO, LS and CP damage states. The results are illustrated in Figure 4.3 and Figure 4.4 and the fragility parameters (mean and standard deviation of ln(PGV)) are given in Table 4.4. It can be seen from fragility curves that subject buildings are collapsed at very low IM levels and they are explicitly vulnerable under future earthquakes. Although both building types reach collapse state at low PGV values, the Type-2 buildings are more vulnerable. In almost all cases, the exceedance of the IO limit of the buildings is due to the beams. That is, although columns do not reach the IO limit yet, the buildings exceed the IO limit since 20% of the beams exceeds the IO limit. For the exceedance of the LS limit of the buildings, both columns and beams are effective. But the performance of columns mostly determines whether the building exceed the CP limit or not. In general, failure is observed in the first story. Among two limit state definitions, in all cases, strain limits calculated according to the TBEC (2018) give more conservative fragility curves when compared to the chord rotation limits calculated according to the Eurocode 8 (2005). In general, LS fragility curves are close to the CP fragility curves. The main reason is the way for the determination of the global performance of the buildings used in this study (see Chapter 4.1.3). When only columns are considered, the only difference between the DS of LS and CP is that the LS performance level does not allow the sum of shear forces of the columns in the advanced damage region to be more than 20% of the story shear force at each story. When columns are dominant for buildings to reach the DS of the LS and CP, the resultant LS fragility curves are close to the CP fragility curves. Another reason for this situation is that the LS limits of structural members are close to the CP limit rather than the IO limit, especially for the Type-1 buildings. Therefore, the probability of the subject buildings to exceed LS performance level is close to the exceedance probability of the CP performance level. Note that Model14 reaches the CP performance level at very low IM levels since the building has long span dimensions in an axis. Therefore, it is not possible to fit the IO and LS fragility curves for that model.

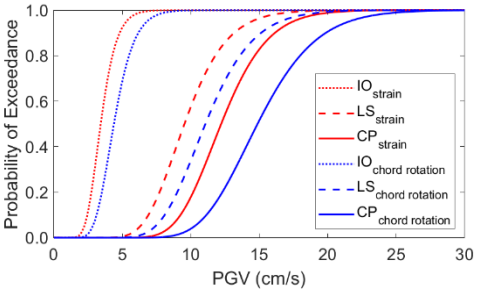

(a) Model01 (Type-1)

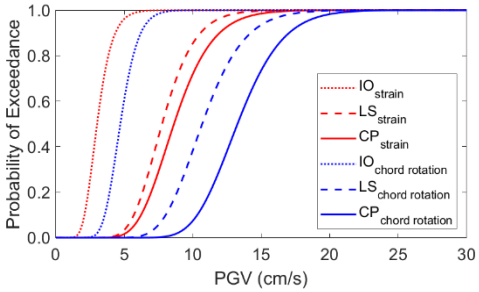

(b) Model02 (Type-2)

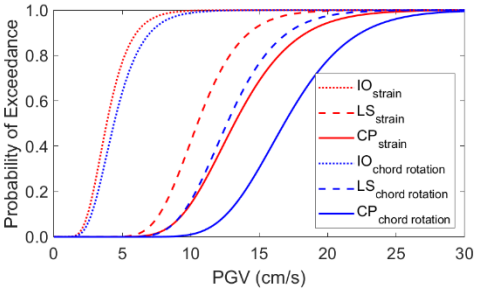

(c) Model03 (Type-1)

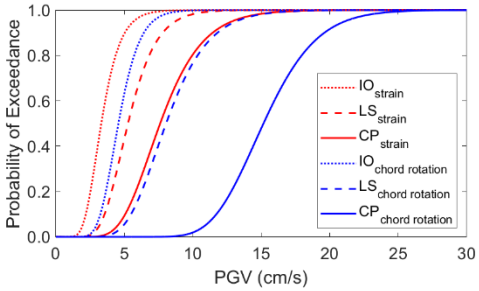

(d) Model04 (Type-2)

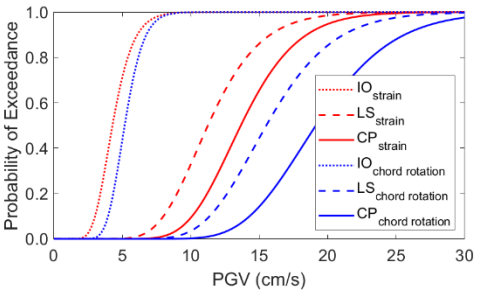

(e) Model05 (Type-1)

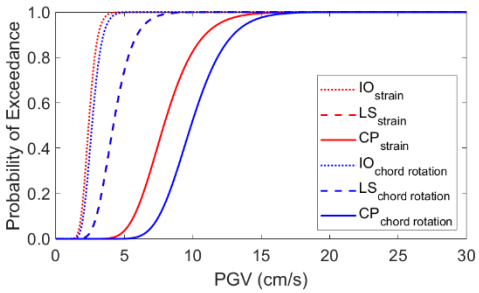

(f) Model06 (Type-2)

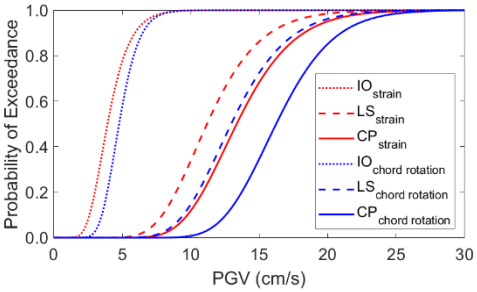

(g) Model07 (Type-1)

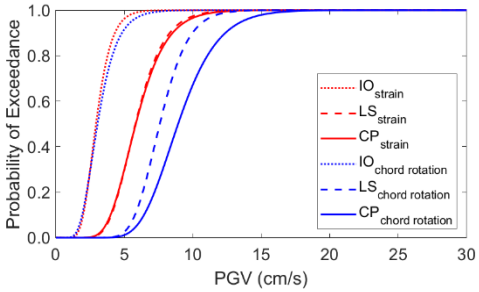

(h) Model08 (Type-2)

Figure 4.3. Fragility curves of 16 building models. cont.

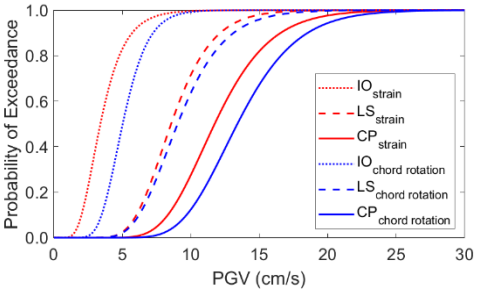

(i) Model09 (Type-1)

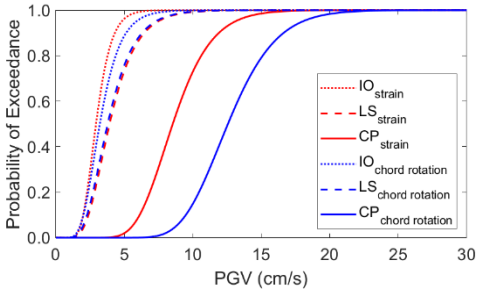

(j) Model10 (Type-2)

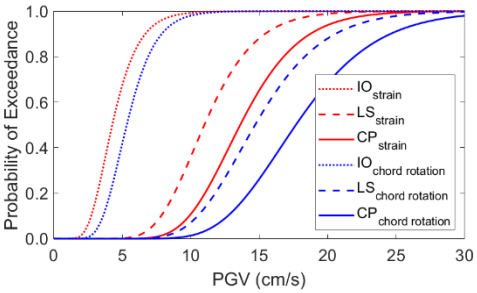

(k) Model11 (Type-1)

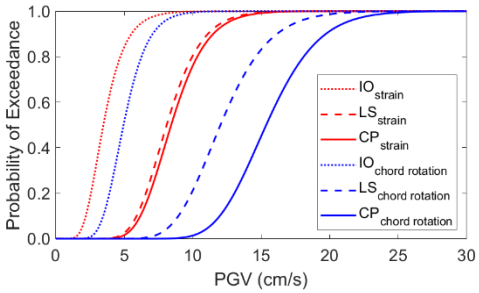

(l) Model12 (Type-2)

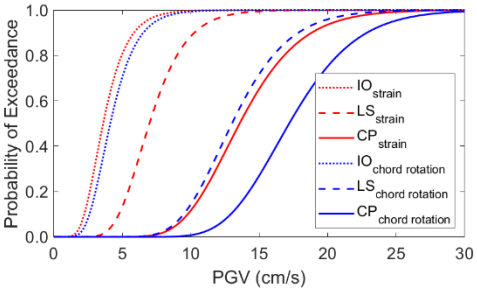

(m) Model13 (Type-1)

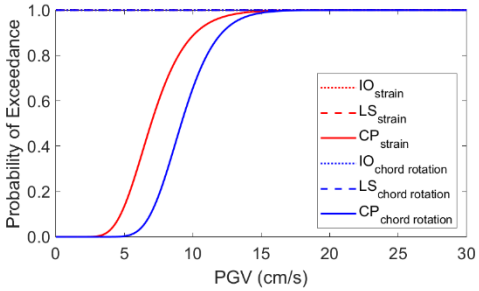

(n) Model14 (Type-2)

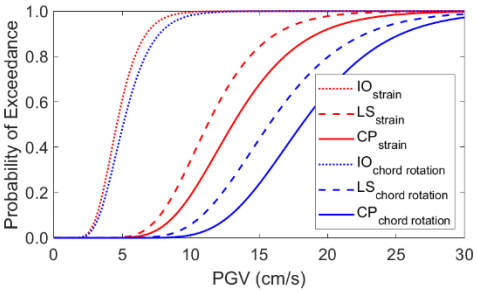

(o) Model15 (Type-1)

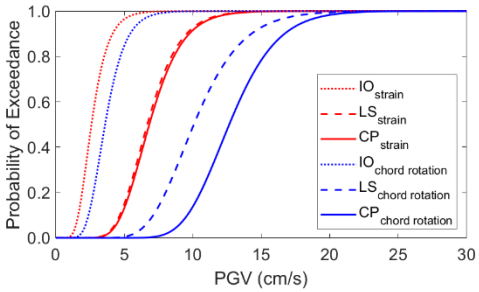

(p) Model16 (Type-2)

Figure 4.4. Fragility curves of 16 building models.

Table 4.4. Fragility parameters of 16 building models (limit state: strain).

Model ID	IO		LS		CP	
	μ	β	μ	β	μ	β
01	1.230	0.265	2.255	0.252	2.503	0.217
02	1.101	0.287	2.048	0.241	2.155	0.255
03	1.349	0.350	2.350	0.240	2.579	0.262
04	1.199	0.326	1.661	0.307	2.030	0.318
05	1.454	0.276	2.420	0.266	2.614	0.236
06	0.870	0.202	1.433	0.272	2.065	0.253
07	1.365	0.322	2.415	0.269	2.592	0.245
08	1.075	0.301	1.759	0.281	1.764	0.296
09	1.222	0.407	2.147	0.273	2.463	0.269
10	1.075	0.301	1.366	0.390	2.144	0.260
11	1.450	0.350	2.397	0.264	2.611	0.249
12	1.244	0.362	2.091	0.247	2.131	0.243
13	1.280	0.378	1.943	0.301	2.608	0.255
14	-	-	-	-	1.939	0.300
15	1.525	0.301	2.419	0.288	2.570	0.303
16	0.955	0.363	1.898	0.279	1.920	0.278

Table 4.5. Fragility parameters of 16 building models (limit state: chord rotation).

Model ID	IO		LS		CP	
	μ	β	μ	β	μ	β
01	1.478	0.266	2.404	0.244	2.700	0.225
02	1.549	0.216	2.369	0.224	2.585	0.195
03	1.479	0.367	2.537	0.235	2.823	0.225
04	1.519	0.267	2.086	0.299	2.719	0.201
05	1.642	0.209	2.742	0.242	2.952	0.228
06	0.969	0.215	1.433	0.272	2.290	0.212
07	1.561	0.240	2.561	0.246	2.787	0.200
08	1.113	0.360	2.027	0.213	2.189	0.255
09	1.614	0.286	2.201	0.291	2.595	0.253
10	1.166	0.367	1.331	0.397	2.531	0.219
11	1.671	0.306	2.688	0.262	2.872	0.258
12	1.598	0.279	2.487	0.230	2.732	0.195
13	1.415	0.360	2.565	0.247	2.844	0.223
14	-	-	-	-	2.215	0.220
15	1.622	0.329	2.755	0.289	2.896	0.264
16	1.279	0.321	2.310	0.272	2.539	0.216

In addition, the fragility curves that show the probability of exceedance of the IO, LS, and CP are illustrated separately and the buildings having the same typology are included in the same figure (see Figure 4.5, Figure 4.6 and Figure 4.7). It is observed that there is considerable variability between fragility curves of the buildings that are in the same typology. Therefore, consideration of variabilities in structural models makes a huge impact on the exceedance probabilities of damage states.

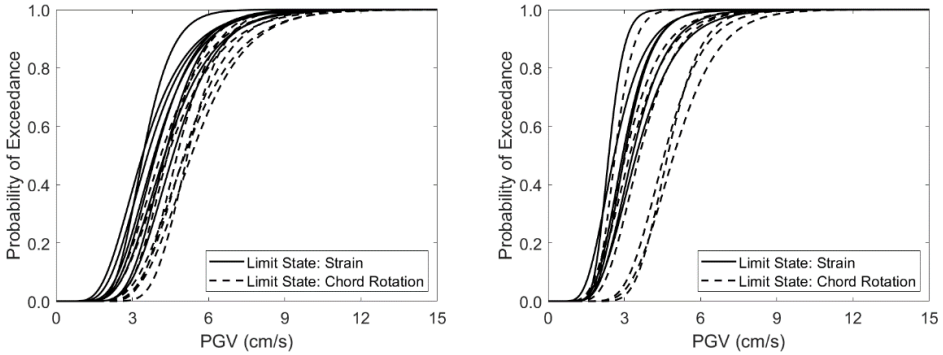

(a) Type-1 buildings (b) Type-2 buildings

Figure 4.5. IO fragility curves of two building types.

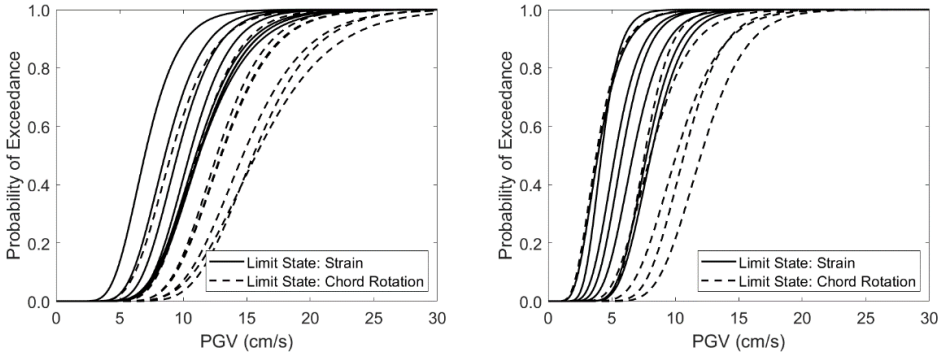

(a) Type-1 buildings (b) Type-2 buildings

Figure 4.6. LS fragility curves of two building types.

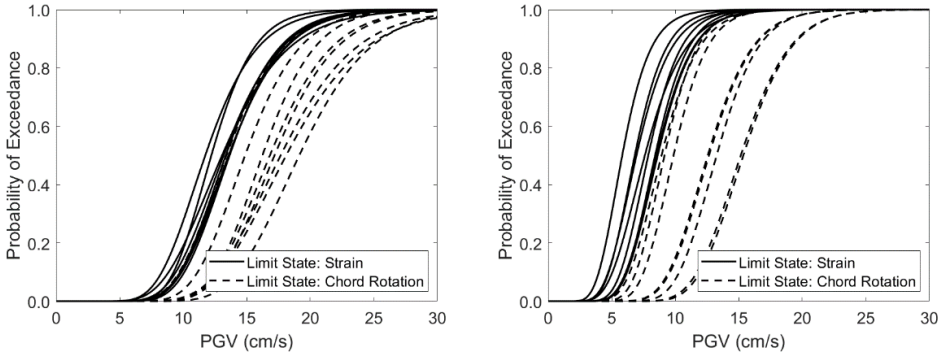

(a) Type-1 buildings (b) Type-2 buildings

Figure 4.7. CP fragility curves of two building types.

Finally, fragility curves of two building types are generated with 95% confidence intervals and illustrated in Figure 4.8. Two limit state definitions and all the building models that are in the same typology are included in the same fraction for the generation of fragilities for subject building stock. Their parameters can be seen in Table 4.6. The TBEC (2018) states that the target performance level for existing residential RC buildings is LS under earthquakes with DD-2 level (earthquakes having 10% exceedance probability in 50 years). According to the hazard curves illustrated in Chapter 2.4.3, the PGV values of earthquakes having 10% exceedance probability in 50 years is 25 cm/s in KAAH15 (Kale et al., 2015), 31 cm/s in ASB14 (Akkar et al., 2014) and 29 cm/s in CY14 (Chiou and Youngs, 2014). The below fragility curves show that all no-code mid-rise RC buildings in İstanbul reach collapse under the earthquakes having the 475-year return period.

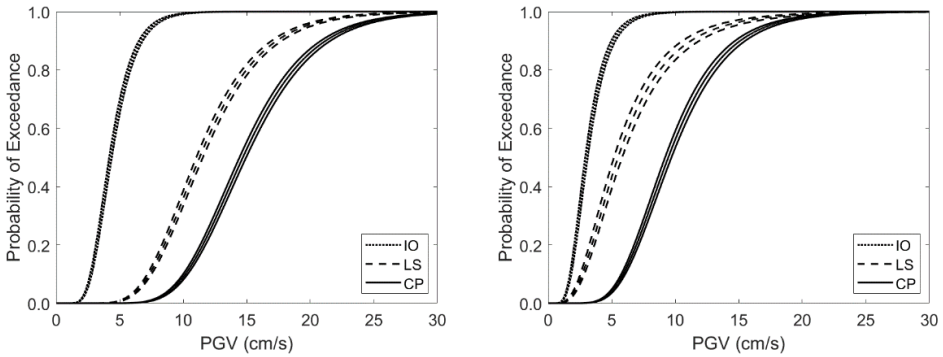

(a) Type-1 buildings (b) Type-2 buildings

Figure 4.8. Fragility curves of two building types with 95% confidence levels.

Table 4.6. Fragility parameters with 95% confidence levels of two building types.

	Building Type	IO		LS		CP	
		μ	β	μ	β	μ	β
Mean	Type-1	1.454	0.346	2.424	0.336	2.687	0.286
Upper Bound		1.478	0.346	2.447	0.336	2.705	0.286
Lower Bound		1.430	0.346	2.401	0.336	2.670	0.286
Mean	Type-2	1.104	0.416	1.706	0.557	2.247	0.366
Upper Bound		1.137	0.416	1.763	0.557	2.273	0.366
Lower Bound		1.070	0.416	1.645	0.557	2.220	0.366

4.4. Determination of MIDR Limits

Interstory drift ratios and lateral deformations are mostly used performance measures in seismic analysis of the structures. MIDR is a good indicator of building damages through stories under lateral loads. For performance assessment of structures via NRHA, the cyclic behavior of structural members highly imprints the overall response of the building. Therefore, determination of the performance levels of the buildings based on the structural member performances is considered to be the most realistic way and fragility curves of building models are generated based on local member performances in Chapter 4.2. However, when large building stocks are examined for fragility generation, the time-efficient ways may become important since a large number of building models is needed. There is no doubt that monitoring structural member performances increases the cost of analysis since hundred of thousands of data files and dozens of gigabytes of data are created at the end of the analysis. For this reason, using MIDR for performance assessment is practical when compared to the monitoring structural member performance. In this study, fragility curves of two building types are generated using MIDR limits and the resultant curves with different damage measures are compared.

MIDR limits of two building types are determined by use of IO, LS, and CP limits of structural members. For this purpose, at each increment of a single IDA study, the performance level of the buildings is determined based on the regulations stated in Chapter 4.1.3. MIDR values at transition points from one performance level to the other are used for the determination of the IO, LS, and CP limits in terms of MIDR. For example, the IO limit is defined as the MIDR value at the increment of a single record IDA study where the

IO limit is exceeded. Similarly, LS and CP limits in terms of MIDR are determined. This process is carried out for all 800 single-record IDA studies by use of 16 building models and 25 ground motion pairs. The distribution of MIDR limit values of IO, LS, and CP is illustrated in Figure 4.10 and Figure 4.11. Note that Type-1 and Type-2 buildings are evaluated separately since there a considerable difference between two building types in terms of response statistics. Therefore, in this section, MIDR limits corresponding to strain limits from the TBEC (2018) and chord rotation limits from the Eurocode 8 (2005) are calculated for two building types separately.

It can be observed from histograms in Figure 4.9 and Figure 4.10 that MIDR limits corresponding to strain and chord rotation limits show a disperse behavior due to the variety in structural models and ground motion records. As expected, Type-2 buildings reach IO, LS, and CP performance levels at lower MIDR values since they have less deformation capacity. In addition, just like fragility curves illustrated in Figure 3.3 and Figure 4.4, MIDR limits corresponding to strain limits from TBEC (2018) are conservative when compared to the ones related to chord rotation limits from Eurocode 8 (2005). Mean and standard deviation of the IO, LS, and CP limits in terms of MIDR are determined and illustrated in Table 4.7 and Table 4.8. By use of mean values, fragility curves are generated for each building type and illustrated in Figure 4.11. In the same figure, the fragility curves generated using local member performances are also illustrated for the comparison of the results. Their parameters are shown in Table 4.9. It can be seen from Figure 4.11 that fragility curves generated for both limit state definitions are more or less the same. As a result, using MIDR limits is more practical when compared to strain and chord rotation limits. If a suitable MIDR limit is used, the resultant fragility curve is very similar to the one generated using local member performances.

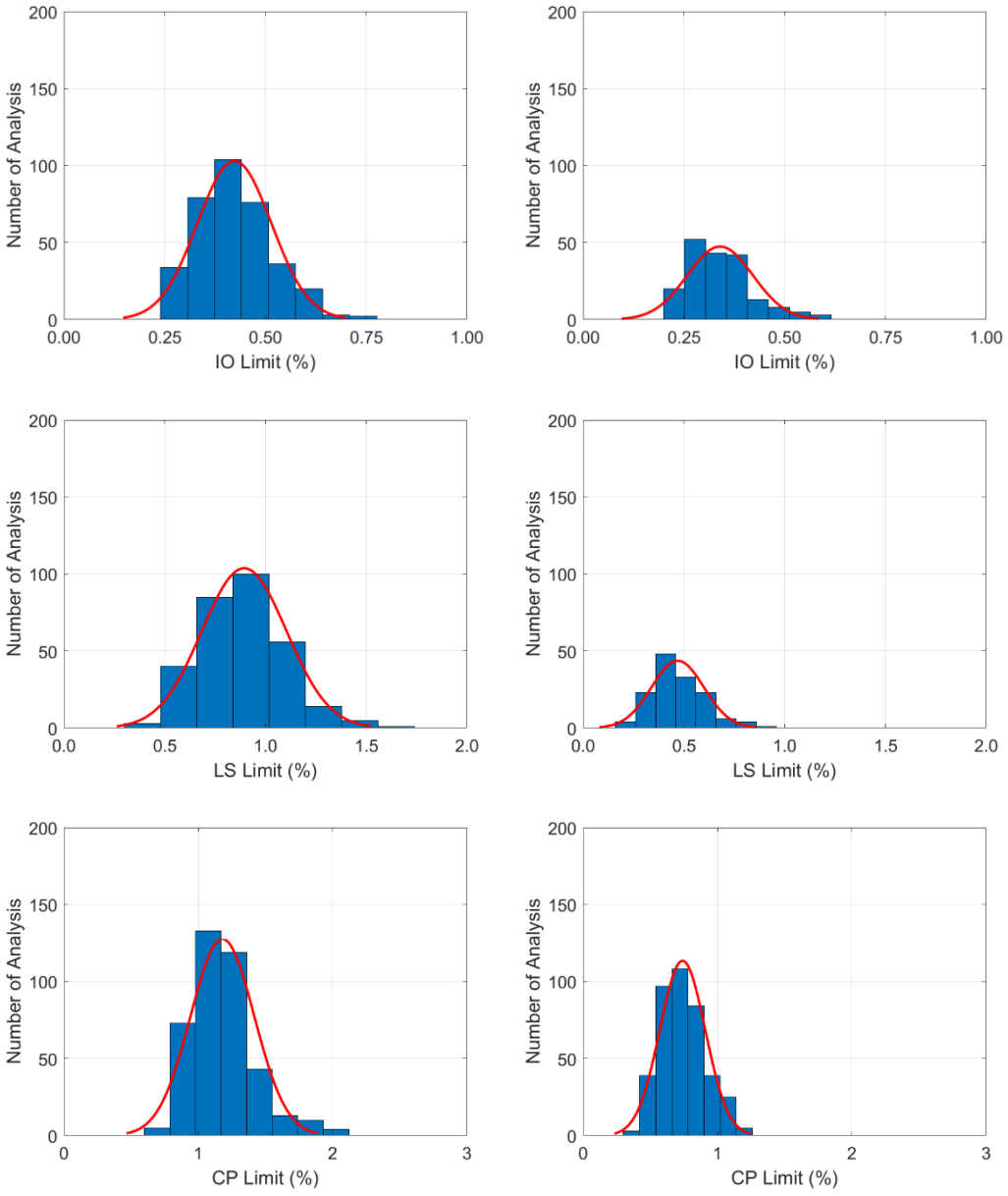

(a) Type-1 buildings (b) Type-2 buildings

Figure 4.9. Distribution of MIDR limits corresponding to strain limits from TBEC (2018) calculated for no code mid-rise RC MRF buildings.

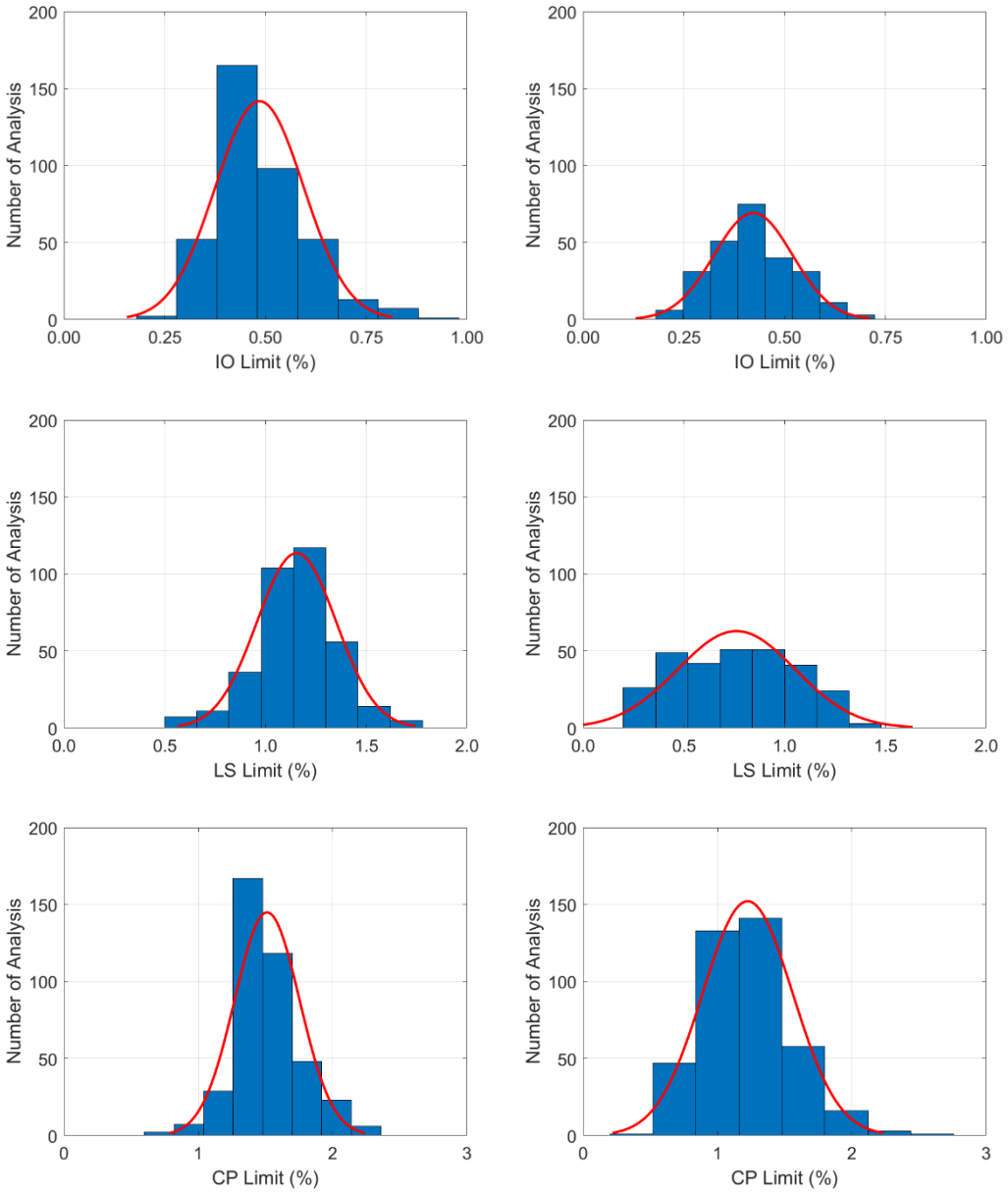

(a) Type-1 buildings (b) Type-2 buildings

Figure 4.10. Distribution of MIDR limits corresponding to chord rotation limits from Eurocode 8 (2005) calculated for no code mid-rise RC MRF buildings.

Table 4.7. MIDR limits (%) corresponding to strain limits from TBEC (2018).

	Mean (%)			Standard Deviation (%)		
Building Type	IO	LS	CP	IO	LS	CP
Type-1	0.42	0.89	1.18	0.09	0.21	0.24
Type-2	0.34	0.47	0.74	0.08	0.13	0.17

Table 4.8. MIDR limits (%) corresponding to chord rotation limits from Eurocode 8 (2005).

	Mean (%)			Standard Deviation (%)		
Building Type	IO	LS	CP	IO	LS	CP
Type-1	0.49	1.16	1.51	0.11	0.20	0.24
Type-2	0.42	0.76	1.23	0.10	0.29	0.34

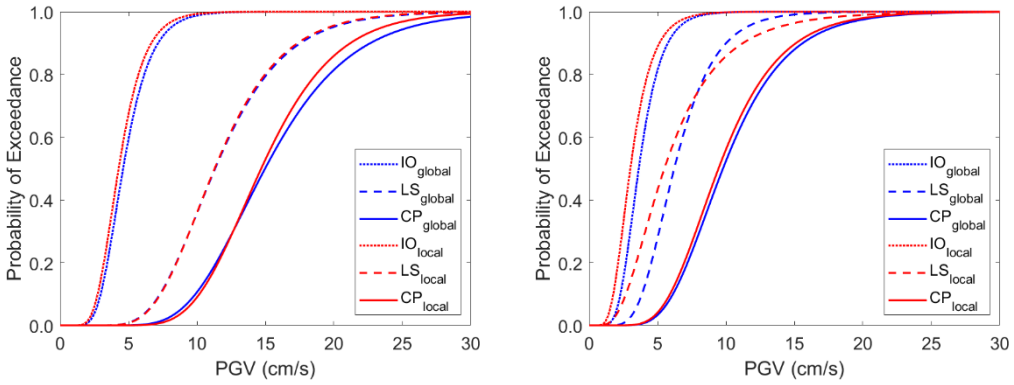

(a) Type-1 buildings (b) Type-2 buildings

Figure 4.11. Comparison of fragility curves of two building types generated using global damage measure (MIDR) and local damage measure (strain and chord rotation of structural members).

Table 4.9. Fragility parameters of two building types generated using global damage measure (MIDR) and local damage measure (strain and chord rotation of structural members).

DS Definition	Building Type	IO		LS		CP	
		μ	β	μ	β	μ	β
Strain and Rotation	Type-1	1.454	0.346	2.424	0.336	2.687	0.286
MIDR		1.528	0.344	2.427	0.342	2.707	0.323
Strain and Rotation	Type-2	1.104	0.416	1.706	0.557	2.247	0.366
MIDR		1.290	0.359	1.828	0.372	2.281	0.365

5. CONCLUSION

5.1. Major Outcomes and Observations

This study has been carried out to provide analytical fragility functions for no-code mid-rise reinforced concrete frame-type buildings for İstanbul that partially encompass the no-code building vulnerability in Turkey. The resulting fragility curves strongly depend on the variation of structural models within the same building typology. Therefore, consideration of different types of structural plan is essential for a proper fragility assessment of building stocks. It is a well-known fact that in order to observe full inelastic response ranges of buildings under seismic actions, a large suite of suitable earthquake records with different time and pattern characteristics should be applied to the building models. In addition, change in the definition of limit states highly imprints the results of analytical fragility analysis. To illustrate, for subject building models, consideration of strain limits of the structural components gives conservative fragility curves when compared to the ones developed using chord rotation limits. As a result, consideration of uncertainties in (a) structural models, (b) earthquake records and (c) limit state definitions makes an enormous effect on the loss assessment of building stocks. To this respect, a backbone fragility curve by up and down scaling of a central model is an obligation for the estimation of exceedance probability of damage states of building stocks.

Among analysis types, IDA (Vamvatsikos and Cornell, 2002) gives ideal and practical solutions for the estimation of inelastic response of buildings under an increasing intensity level of earthquakes. Results of 9535 NRHA in the form of IDA show that PGV correlates better with inelastic displacement demands when compared to other common ground motion indices. When IDA curves are converted to the capacity curves, i.e., EDPs of maximum base shear coefficient and MIDR are plotted together, the resultant median curves are mostly similar to the ones obtained from pushover analysis because most of the subject buildings are first-mode dominant. However, pushover analysis generally underestimates building capacities of subject buildings. Since the energy and frequency content, as well as time and pattern of the seismic actions are considered in NRHA, it is the most realistic analysis type when 3-D models are used. But the results show that traditional

pushover analysis can be considered as a practical way for response prediction of mid-rise buildings.

NRHA results of 16 building models reflecting about 800 existing no-code mid-rise RC MRF buildings in the Zeytinburnu distinct in İstanbul show that subject building stock is highly vulnerable under future earthquakes. The existing buildings are constructed before 1980 with traditional techniques and poor controlling mechanism, i.e., structural detailing of them do not satisfy an earthquake design code. Therefore, subject buildings are named as no-code buildings. Poor detailing of structural members of no-code buildings results reaching collapse state at earlier stages of IDA. That is, the buildings exceed the CP performance level at low IM levels. To illustrate, according to the TBEC (2018), the minimum performance level under earthquakes having 475-year return period is LS for existing RC buildings. But all building models reach collapse state under earthquakes having 475-year return period.

The Type-2 buildings are more vulnerable and have less deformation capacity since their structural components have unconfined concrete and the amount of longitudinal reinforcement is less in Type-2 buildings. Considering mean values, while the Type-1 buildings reach collapse limit at a MIDR value of 1.35%, the Type-2 buildings reach the limit at 0.99% MIDR value. In 16 building models, the IO limit is mostly exceeded due to the beams. In the early stages of the IDA, while columns stay below the IO limit, 20% of the beams exceeds the limit and so, the building is accepted to exceed the limit. There is no such distinction for the LS limit, i.e., columns or beams can be effective for buildings to exceed the LS limit. However, in most cases, the CP limit of the buildings is exceeded due to the columns exceeding the limit.

5.2. Recommendations for Future Studies

This study is limited to 5-story RC buildings reflecting no-code mid-rise building stock in İstanbul which is the biggest metropolis in Turkey. Although the construction practice is similar to the other crowded cities of this country, inventory study can be amplified considering the no-code building database of the other cities. In addition, similar studies can be conducted by use of other RC building types like low-rise or high-rise

buildings with different structural systems like shear wall or dual systems containing combinations of MRF and shear walls.

Since there is no information about the reinforcement detailing of subject stock, the minimum amount of reinforcement suggested in the TEC (1975) is used in the structural components of half of the building models. For the other half, less amount of reinforcement is used. These assumptions are accepted to reflect the detailing of the no-code building stock. But building databases having reinforcement detailing of structural components can be used for better estimation of building vulnerability. In addition, consideration of infill walls, lap-splice deficiencies, the reinforcement corrosion and poor detailing of the beam-column joints can be considered in modelling part since these issues are quite critical challenges related to response prediction of seismically deficient building stocks.

REFERENCES

ACI-318, "American Concrete Institute", *Building Code Requirements for Reinforced Concrete*, Detroit, 1963.

ACI-318, "American Concrete Institute", *Building Code Requirements for Structural Concrete*, Detroit, 1999.

Akkar, S. and Özen, Ö., "Effect of Peak Ground Velocity on Deformation Demands for SDOF Systems", *Earthquake Engineering and Structural Dynamics*, 34, 1551–1571, 2005.

Akkar, S., Sucuoğlu, H., and Yakut, A., "Displacement-Based Fragility Functions for Low and Mid-Rise Ordinary Concrete Buildings" *Earthquake Spectra*, 21(4):901–927, 2005.

ASCE/SEI Standard 41-06, "Seismic Rehabilitation of Existing Buildings", *American Society of Civil Engineers*, Reston, Virginia, USA, 2006.

Ay, B.Ö., and Erberik, M.A., "Vulnerability of Turkish Low-Rise and Mid-Rise Reinforced Concrete Frame Structures", *Earthquake Engineering*, 12(S2):2-11, 2008.

Baker, J. W., "Probabilistic Structural Response Assessment using Vector-Valued Intensity Measures", *Earthquake Engineering & Structural Dynamics*, 36(13), 1861-1883, 2007.

Baker, J. W., "Fitting Fragility Functions to Structural Analysis Data using Maximum Likelihood Estimation, *Standford University*, 2011.

Barani, S., Spallarossa, D., & Bazzurro, P., "Disaggregation of Probabilistic Ground-Motion Hazard in Italy", *Bulletin of the Seismological Society of America*, 99(5), 2638-2661, 2009.

Deierlein, Gregory G., Reinhorn, Andrei M., & Willford, Michael R., "Nonlinear structural analysis for seismic design", *NEHRP seismic design technical brief*, 4: 1-36, 2010.

Dolağan, İ., "Development of Peak Ground Acceleration (PGA) Based Pre-Code Reinforced Concrete Frame Building Fragilities for İstanbul", *M.Sc. Thesis, Department of Earthquake Engineering, Bogazici University*, İstanbul, Turkey, 2019.

Erberik, M. A., "Generation of Fragility Curves for Turkish Masonry Buildings Considering In-Plane Failure Modes", *Earthquake Engineering & Structural Dynamics*, 37(3), 387-405, 2008.

Erberik, M. A., & Elnashai, A. S., "Fragility Analysis of Flat-Slab Structures", *Engineering Structures*, 26(7), 937-948, 2004.

Erdik, M., "Earthquake Risk Assessment", *Bulletin of Earthquake Engineering*, 15(12), 5055-5092., 2017.

European Committee for Standardization, "Eurocode 8: Design of Structures for Earthquake Resistance, Part 3: Strengthening and Repair of Buildings", *Eurocode 8*, Brussels, 2005.

FEMA-356, "NEHRP Prestandard and Commentary for the Seismic Rehabilitation of Buildings", *Federal Emergency Management Agency*, Washington, DC., 2000.

FEMA-P-58-1, "Seismic Performance Assessment of Buildings", *Federal Emergency Management Agency*, Washington, DC., 2012.

Fragiadakis, M., & Vamvatsikos, D., "Qualitative Comparison of Static Pushover versus Incremental Dynamic Analysis Capacity Curves", *In Proceedings of the 7th Hellenic National Conference on Steel Structures*, 2011.

Ghobarah, A., Aly, N. M., & El-Attar, M., "Seismic Reliability Assessment of Existing Reinforced Concrete Buildings", *Journal of Earthquake Engineering*, 2(04), 569-592, 1998.

Grünthal, G., "European Macroseismic Scale 1998", *European Seismological Commission (ESC)*, 1998.

Haselton, C. B., Whittaker, A. S., Hortacsu, A., Baker, J. W., Bray, J., & Grant, D. N., "Selecting and Scaling Earthquake Ground Motions for Performing Response-History Analyses", *In Proceedings of the 15th World Conference on Earthquake Engineering 4207-4217, Earthquake Engineering Research Institute*, 2012.

Kırçıl, M.S., and Polat, Z., "Fragility Analysis of Mid-Rise RC Frame Buildings", *Engineering Structures*, 28(9):1335–1345, 2006.

Kwon, O. S., & Elnashai, A., "The Effect of Material and Ground Motion Uncertainty on the Seismic Vulnerability Curves of RC Structure", *Engineering Structures*, 28(2), 289-303, 2006.

Mander, J. B., Priestley, M.J.N., and Park, R., "Theoretical Stress-Strain Model for Confined Concrete", *Structural Engineering*, Vol. 114, Issue 8, 1988.

Masjed-Jamei, Mohammad, M. R. Eslahchi, and Mehdi Dehghan, "On Numerical Improvement of Gauss–Radau Quadrature Rules", *Applied Mathematics and Computation*, 168.1, 51-64, 2005.

Medvedev, S. V., & Sponheuer, W., "Scale of Seismic Intensity", *In Proc. IV World Conference of the Earthquake Engineering*, Santiago, Chile, A-2 (pp. 143-153), 1969.

McKay, M. D., Beckman, R. J., & Conover, W. J., "Comparison of Three Methods for Selecting Values of Input Variables in the Analysis of Output from a Computer Code", *Technometrics*, 21(2), 239-245, 1979

Menegotto, M., & Pinto, P., "Method of Analysis for Cyclically Loaded Reinforced Concrete Plane Frames Including Changes in Geometryand Non-elastic Behavior of Elements Under Combined Normal Force and Bending. Proceedings", *IABSE Sympoium on Resistance and Ultimate Deformability of Structures Acted on by Well-Defined Repeated Loads*, 1973.

Molas, G., Rahnama M. & Seneviratna, P., "On the Correlation of Ground Motion Indices to Damage of Structural Models", *13th World Conference on Earthquake Engineering*, Canada, 2004.

National Institute of Building Sciences, "Direct Physical Damage – General Building Stock", *HAZUS-MH Technical Manual, Federal Emergency Management Agency*, Washington, D.C., 2004.

NBCC, "National Building Code of Canada", *Nationd Research Council of Canada*, Ottawa, 1995.

Park, Y. J., & Ang, A. H. S., "Mechanistic Seismic Damage Model for Reinforced Concrete", *Journal of Structural Engineering*, 111(4), 722-739., 1985.

Rossetto, T., & Elnashai, A., "Derivation of Vulnerability Functions for European-type RC Structures based on Observational Data", *Engineering Structures*, 25(10), 1241-1263, 2003.

Rossetto, T., & Elnashai, A., "A New Analytical Procedure for the Derivation of Displacement-Based Vulnerability Curves for Populations of RC Structures", *Engineering Structures*, 27(3), 397-409, 2005.

Rubenstein, R. Y., "Simulation and the Monte Carlo Method", New York: John Wiley, 1981.

SAC Joint Venture, "Recommended Design Criteria for New Steel Moment-Frame Buildings", *FEMA-350*, Washington, DC., 2000a.

Sadraddin, H. & Shao, Xi. & Hu, Y. “Fragility Assessment of High-Rise Reinforced Concrete Buildings Considering the Effects of Shear Wall Contributions”, *The Structural Design of Tall and Special Buildings*, 25:1089-1102, 2016.

SEAOC, “Recommended Lateral Force Requirements and Commentary”, *Structural Engineers Association of California*, 1990.

SEAOC, “Recommended Lateral Force Requirements and Commentary”, *Structural Engineers Association of California*, 1999.

Singhal, A., & Kiremidjian, A. S., “Method for Probabilistic Evaluation of Seismic Structural Damage”, *Journal of Structural Engineering*, 122(12), 1459-1467, 1996.

Shome, N. and Cornell, C. A., “Probabilistic Seismic Demand Analysis of Nonlinear Structures”, *Report No. RMS-35, RMS Program, Stanford University*, Stanford, CA, 1999.

Sucuoglu, H., & Erberik, M. A., “Influence of Ground Motion Intensity Parameters on Elastic Response Spectra”, *In Proceedings of the 11th European Conference on Earthquake Engineering*, Paris, 1998.

Turkish Building Earthquake Code, *Specification for Design of Buildings in Disaster Areas*, Disaster and Emergency Management Presidency Government of Republic of Turkey, 2018.

Turkish Earthquake Code, *Specification for Structures to be Built in Disaster Areas*, Ministry of Public Works and Settlement Government of Republic of Turkey, 1975.

Turkish Earthquake Code, *Specification for Structures to be Built in Disaster Areas*, Ministry of Public Works and Settlement Government of Republic of Turkey, 1998.

Turkish Earthquake Code, *Specification for Structures to be Built in Disaster Areas*, Ministry of Public Works and Settlement Government of Republic of Turkey, 2007.

Vamvatsikos, D., and Cornell, C.A., “Incremental Dynamic Analysis”, *Earthquake Engineering and Structural Dynamics*, 31:491–514, 2002.